Dziewonski, A., Wilkens, R., Firth, J., et al., 1992
Proceedings of the Ocean Drilling Program, Initial Reports, Vol. 136

4. SITE 842[1]

Shipboard Scientific Party[2]

HOLE 842A

Date occupied: 3 March 1991

Date departed: 4 March 1991

Time on hole: 14 hr 30 min

Position: 19°20.18′N, 159°5.33′W

Bottom felt (rig floor; m, drill-pipe measurement): 4441.0

Distance between rig floor and sea level (m): 10.77

Water depth (drill-pipe measurement from sea level, m): 4430.2

Total depth (rig floor; m): 4450.50

Penetration (m): 9.5

Number of cores (including cores with no recovery): 1

Total length of cored section (m): 9.5

Total core recovered (m): 9.66

Core recovery (%): 102

Oldest sediment cored:
Depth (mbsf): 9.66
Nature: Radiolarian- and ash-rich clay/clayey silt
Age: Quaternary
Measured velocity (km/s): 1.483

HOLE 842B

Date occupied: 4 March 1991

Date departed: 5 March 1991

Time on hole: 1 day 10 hr 15 min

Position: 19°120.18′N, 159°5.33′W

Bottom felt (rig floor; m, drill-pipe measurement): 4662.4

Distance between rig floor and sea level (m): 10.77

Water depth (drill-pipe measurement from sea level, m): 4430.4

Total depth (rig floor; m): 4609.0

Penetration (m): 221.2

Number of cores (including cores with no recovery): 10

Total length of cored section (m): 72.3

Total core recovered (m): 35.65

Core recovery (%): 49.3

Oldest sediment cored:
Depth (mbsf): 72.3
Nature: Chert fragments bound with clay
Age: late Cretaceous
Measured velocity (km/s): N/A

Comments: Between Cores 136-842B-8X and -9X (58.1–106.0 mbsf) and between Cores 136-842B-9X and -10X (115.7–163.3 mbsf) drilled, but not cored. Drilled below Core 136-842B-10X from 167.8–221.2 mbsf.

HOLE 842C

Date occupied: 5 March 1991

Date departed: 7 March 1991

Time on hole: 1 day 1 hr 30 min

Position: 19°20.18′N, 159°5.39′W

Bottom felt (rig floor; m, drill-pipe measurement): 4441.2

Distance between rig floor and sea level (m): 10.77

Water depth (drill-pipe measurement from sea level, m): 4430.4

Total depth (rig floor; m): 4678.9

Penetration (m): 237.7

Number of cores (including cores with no recovery): 1

Total length of cored section (m): 96.4

Total core recovered (m): 0.88 (see comments, below)

Core recovery (%): 0.9

Comments: Hole 842C was drilled to 141.3 mbsf, then washed down to 237.7 mbsf recovering one wash core (0.88 m).

Principal results: The principal objective of operations at Site 842 was the installation of a reentry cone on the seafloor and the casing of a hole to basement for use as a test site for the Ocean Seismic Network. Site 842 was located on the shoulder of a low northwest–southeast-trending abyssal ridge. Pre-drilling site survey data indicated a total relief of approximately 75 m (4475–4400 m uncorrected depth).

Three holes were drilled at Site 842, with a total depth (TD) of 237.7 mbsf. APC coring extended to 35.7 mbsf, and drilling with intermittent XCB and wash cores extended from 35.7 to TD. The principal lithologies recovered were:

Lithologic Unit I (0–19.9 mbsf): Quaternary to Pliocene (?) silty clays, clayey silts, and clays. All of the sediments of this unit contain variable amounts of volcanic ash and radiolarians. Ash layers are fresh at the top of the interval and altered almost totally to clay and zeolite at the bottom.

Lithologic Unit II (19.9–35.7 mbsf): Middle Miocene to late Eocene clay and claystone with altered ash. Nodules of silica-cemented claystone are also present.

Lithologic Unit III (nominally 35.7–T.D.): This unit is a "catch-all" for the cherts and small samples of Santonian nannofossil ooze (approximately 164 mbsf) returned in several wash core barrels and during attempts to cut regular core. The cherts are varicolored, and contain both opal-CT and, deeper in the section, quartz.

The volcanic ash in Core 136-842A-1H is dispersed throughout the section and is also present as discrete layers. The ash layers are not seen at equivalent levels in the cores of Hole 842B — one of several puzzles in correlating the shallow sediments sampled at these adjacent holes. Well-developed ash horizons in Core 136-842A-1H contain fresh glass as well as minerals that may have been deposited as the result of explosive Hawaiian eruptions. All of the fresh, distinct ash layers are younger than

[1]Dziewonski, A., Wilkens, R., Firth, J., et al., 1992. *Proc. ODP, Init. Repts.,* 136: College Station, TX (Ocean Drilling Program).
[2]Shipboard Scientific Party is as given in the list of participants preceding the contents.

1.4 Ma. Ash horizons are seen deeper in the section at Hole 842B, but they are considerably altered. The origins of these ash layers are less well understood.

Paleomagnetic data from Cores 136-842A-1H, 136-842B-1H, and 136-842B-2H were generally in good agreement. The Brunhes-Matuyama boundary was seen at approximately 1.8 mbsf and the Jaramillo event at 4.5 mbsf. There appears to be a meter or more of disturbed section at the top of Core 136-842B-2H. The base of 842B-2H is estimated to be 3.5 Ma based on magnetic reversal stratigraphy. Cores 136-842B-3H and -4H suffer from coring-induced overprinting, which obscures the reversal record.

Physical properties measurements of samples from the APC cores yield normal compaction and shear-strength trends with depth. Local maxima in compressional-wave velocity and bulk density are correlated with the presence of ash layers or increased concentrations of dispersed ash. Correlation between Holes 842A and 842B is relatively good. Of interest is the apparent expansion of the section at Hole 842B relative to Hole 842A, which is best seen in the velocity record. Compressional-wave velocity profiles correlate well near the surface, but become gradually offset up to about 0.5 m at 4 mbsf. Below this level, the offset remains constant.

Core 136-842A-1H contains a 20-cm-thick bed of clayey nannofossil ooze (8.75–8.95 mbsf) with radiolarians, silicoflagellates, diatoms, and sponge spicules intact. A preliminary age of 1.4–1.6 Ma agrees very well with paleomagnetic stratigraphy. Section 136-842A-1H-6 contains as yet undated planktonic foraminifers. Cores 136-842B-3H and -4H contain middle Miocene and late Eocene-middle Miocene icthyoliths, respectively, and Core 136-842B-10X (163.3–167.8 mbsf) yielded Santonian calcareous nannofossils.

The principal failure of operations at Site 842 was our inability to drill and set a reentry cone for later use as a test site of the Ocean Seismic Network. However, the recovery of 46 m of well-documented and dated sediments from an undersampled area of the Pacific seafloor has yielded substantial scientific benefit as well as providing several questions:

1. Both magnetic and biostratigraphic data suggest that sedimentation rates are substantially higher than open ocean North Pacific norms (a rough average of 3 m/Ma for the past 4 m.y.) The surprise is in the lack of a marked increase in volcanic ash sedimentation during the past 1 m.y. of sediment accumulation. The emergence of the Hawaiian Island chain, and in particular the islands of Maui and Hawaii, should be reflected in an increase in airborne ash being deposited at Site 842.

2. Holes 842A and 842B were cored within 10 m of each other, and yet there is a remarkable lack of detailed correlation between the two cored intervals. In particular, ash layers in Core 136-842A-1H are not seen in Cores 136-842B-1H and -2H, and apparent offsets of physical property trends are different from those of the paleomagnetic record.

3. The volume and shallow occurrence of cherts encountered was unexpected. Extremely poor recovery leaves the nature, and for the most part the age, of these cherts as an unknown.

OPERATIONS

Honolulu Port Call

Leg 136 officially began at 0700 hr local time (LT; 1700 hr UTC) on 28 February, when the first line was passed to the dock in Honolulu harbor at Pier 1. The entrance into Honolulu marked the first time that *JOIDES Resolution* had been in a U.S. port since Norfolk, Virginia, in 1985. After customs and immigration officials finished with their formalities, the port-call activities got into high gear, as the port call was scheduled to be only 3 days, and there was a full agenda. Bunkering began first, along with the normal loading of catering supplies and the loading of ODP and UDI ocean and air freight. ODP received 18 bags of bentonite that were left in Townsville, Australia, and shipped to Hawaii, for loading into the bulk tanks. The offloading of cores and other material returning to College Station was handled on the second day of the port call. The pacing activity of the port call was anticipated to be the hull, loadline, and annual inspections by ABS for the vessel; as things went, those inspections were completed in just over 2 days and were accomplished without incident. ODP had prearranged with the U.S. National Oceanic and Atmospheric Administration (NOAA) out of San Diego for the installation of a Shipboard Environmental Acquisition System (SEAS) unit on the bridge of *JOIDES Resolution*. The SEAS unit was to be used to enter weather observations into a computer four times per day and to transmit them back to an East Coast NOAA facility.

The last major task accomplished during the port call was an inspection of the lab stack HVAC system by an engineer from Earl & Wright Engineers out of San Francisco. The purpose of that inspection was to look at what modifications or additions needed to be made to the air conditioning or ventilation of the lab stack to minimize the hazards of any H_2S emissions that may be encountered from cores during Leg 139.

Tours arranged and guided by previous shipboard scientists from the University of Hawaii were held on Friday afternoon, Saturday morning, and Saturday afternoon, 1–2 March. The last tour was finished by 1630 hr on Saturday. On Saturday afternoon the rig crew began to make up the first APC/XCB BHA that would be run at the first site. Normal UDI policy prevents drill collars from being stood back in the derrick during transits, but the transit to the site was only 12 hr, and the weather forecast was favorable. The last line was cast off from the dock at 1830 hr (LT) to begin the voyage to proposed site OSN-1 (Site 842). In the following account, all times given are local.

Transit to Site 842

JOIDES Resolution slowed to 5 kt at 0500 hr (LT) on 3 March, having averaged 11.5 kt for the 120-nmi journey to the site area, and two 80-in.^{3} air guns were deployed for the site survey. A 43-nmi survey, at 6 to 7 kt, was performed and the initial beacon was dropped at 1015 hr, 3 March. After an hour to return to the beacon and lower the thrusters and hydrophones, the dynamic-positioning (DP) system was steady enough to begin making up the BHA and start the trip to the seafloor. The location of the first beacon drop was on a shoulder of an abyssal ridge, and the DP operator was asked to make a boxed excursion in 500-m distances around the beacon as a localized site survey during the pipe trip. The final location was chosen to be 450 m west of the beacon drop, at a corrected PDR depth of 4444 mbrf (meters below rig floor).

Hole 842A

A jet-in test was first performed to establish the 16-in. casing point, with a total penetration of 24 m. The drill string was pulled from the seafloor, and the first APC was shot from 4441.0 mbrf. Core 136-842A-1H recovered 9.66 m of red-brown silty clay with ash layers (Table 1). Because it was unclear that we had recovered the mud line, the drill string was pulled back 3 m, and the ship was offset 10 m to the east to begin Hole 842B.

Hole 842B

Core 136-842B-1H was shot at 0125 hr, 4 March, and recovered 6.3 m of sediments identical to those from 136-842A-1H. Therefore, the mud line was confidently determined to be at 4441.2 mbrf. Four additional APC cores were taken, with Cores 136-842B-1H through -5H coring 35.7 m and recovering 34.99 m. Core 136-842B-5H did not fully stroke, penetrating only 0.9 m and recovering 0.92 m of chert cobbles and cherty silicified mudstone, and requiring 20,000 lb of overpull. XCB coring commenced with Core 136-842B-6X, which penetrated 3.5 m and produced only 0.13 m of cherty rubble. Cores 136-842B-7X and -8X were drilled to full lengths of 9.5 and 9.4 m,

Table 1. Coring summary for Site 842, Holes 842A, B, and C.

Core No	Date March 1991	Time (UTC)	Depth interval (mbsf)	Meters Cored	Meters Recovered	Percent Recovery
Hole 842A						
1H	04	1030	0.0–9.5	9.5	9.66	101.7
			Coring Totals	9.5	9.66	101.7
Hole 842B						
1H	04	1140	0.0–6.3	6.3	6.50	103.0
2H	04	1255	6.3–15.8	9.5	7.93	83.5
3H	04	1400	15.8–25.3	9.5	9.98	105.0
4H	04	1500	25.3–34.8	9.5	9.66	101.0
5H	04	1630	34.8–35.7	0.9	0.92	100.0
6X	04	1830	35.7–39.2	3.5	0.13	3.7
7X	04	2000	39.2–48.7	9.5	0.07	0.7
8X	04	2130	48.7–58.1	9.4	0.09	1.0
	(Drilled)		58.1–106.0			
9X	05	0400	106.0–115.7	9.7	0.00	0.0
	(Drilled)		115.7–163.3			
10X	05	1100	163.3–167.8	4.5	0.37	8.2
			Coring Totals	72.3	35.65	49.3
Hole 842C						
	(Drilled/Washed)		0.0–141.3			
1W	07	0700	141.3–237.7	96.4	0.88	(wash core)
			Coring Totals	0.0	0.00	
			Washing Totals	96.4	0.88	
			Combined Totals	96.4	0.88	

respectively, and recovered a total of only 0.16 m, again chert rubble. The poor recovery prompted the decision to drill ahead with a center bit from the base of Core 136-842B-8X (58.1 mbsf) for four drill-pipe connections to a depth of 106.0 mbsf. The drilling of that interval averaged about 10 m/hr and used a 15-barrel (bbl) sweep of viscous drilling mud to help clean the hole. The recovered center bit showed extreme wear, and the wash barrel contained more chert rubble and fragments. Core 136-842B-9X, taken from 106.0 to 115.7 mbsf, had no recovery. The center bit was once again dropped, and drilling proceeded from 115.7 to 163.3 mbsf, with 60 bbl of drilling mud pumped to help clean the hole of the cherty fragments. The drilling of that interval averaged just over 38 m/hr. Core 136-842B-10X (163.3–167.8 mbsf) produced only 0.37 m of chert rubble. Drilling with a center bit resumed from 167.8 to 192.2 mbsf, and, when pulled, the center bit showed an extreme amount of wear. After replacing the center bit, drilling continued to a depth of 221.2 mbsf. When the center bit was pulled from that depth, it was found that the core barrel, about 20 cm above the center bit, had sheared off because of fatigue and high torque. An XCB core barrel was dropped to determine whether the piece of core barrel and center bit was in the bottom of the hole or if it had been pushed out of the way into the wall of the hole. After the XCB barrel landed, high torquing showed that the debris was still in the hole. Hole 842B had to be abandoned, and the drill pipe was tripped to the surface. Because the object of the exploratory hole at the first site was also to locate the depth of basement to set the 11-3/4-in. casing, it was decided to switch to a 9-7/8-in. rotary bit and an RCB coring assembly.

Hole 842C

During the trip to the seafloor with the drill pipe, the ship was offset 10 m to the east of Hole 842B. The plan before spudding Hole 842C was to drill the hole as quickly as possible and pull the core barrel every 50 m, or as necessary if abnormalities warranted. Hole 842C was spudded at 0530 hr, 6 March, and was drilled to 36 mbsf before the torque became high and the core barrel was pulled. After a new core barrel was in place, drilling proceeded from 36.2 to 141.3 mbsf. Beginning at 60 mbsf, hole torquing was experienced, and drilling-mud sweeps were begun. At the same time, the weather began to cause 2° to 3° rolls. The DP operator was requested to change the heading of the ship, after which the ship's motion subsided considerably, which also helped to reduce the hole torque. The core barrel was pulled after drilling to 141.3 mbsf, and a new core barrel was dropped. Drilling resumed from 141.3 to 237.7 mbsf. The wash core barrel from that interval recovered 0.88 m. With the drill pipe off bottom, after retrieving the wash barrel a new barrel was dropped to cut the first rotary core. Upon attempting to pump the barrel down the drill pipe, the driller found that the flapper valve in the bit could not be opened and that the drill-pipe pressure was already reading 2800–3000 psi. To compound the problem, when the core barrel landed in the BHA it became stuck. The driller picked the string higher off bottom and the hole began to collapse because of the inability to circulate. After considering all of the above, it was decided to abandon Hole 842C, trip the drill pipe to the surface, and offset the ship approximately 1 km northwest to the top of a small elevated seafloor ridge to drill Site 843.

LITHOSTRATIGRAPHY

The sediments recovered at Site 842 have been divided into three lithologic units based on macroscopic core descriptions, smear-slide analyses, thin- section analyses, and X-ray diffraction data. Silty clays and clayey silts with variable amounts of radiolarians and volcanic ash overlie pelagic red clays, which in turn overlie a unit of silica-cemented claystones and cherts (Table 2).

Table 2. Site 842 lithostratigraphic units.

Unit	Lithology	Core Interval (cm)	Depth (mbsf)
I	Radiolarian ashy silty clay, ashy radiolarian clayey silt and clay	842A-1H 842B-1H to 842B-3H-3, 110	0.0–9.5 0.0–19.9
II	Clay/claystone	842B-3H-3, 110 to 842B-5H-CC	19.9–35.7
III	Claystone and chert	842B-6X to -10X 842C-1W	35.7–167.8 141.3–237.7

Unit I (0–19.9 mbsf)

Lithologic Unit I consists of Quaternary to mid-Miocene, dark-brown silty clays, clayey silts and clays, all with variable amounts of volcanic ash and radiolarians. These sediments represent a mixture of pelagic clay and silt-sized ash and siliceous biogenic debris. In general, the silt content decreases downcore. Volcanic ash, discussed in greater detail below, is present both as distinct ash layers and as a dispersed constituent. Silty clays and clays appear homogeneous and structureless, whereas clayey silts tend to be mottled, reflecting the dispersal of ash presumably by bioturbation. The degree of alteration of volcanic ash increases with depth; glass is broken down prior to the crystalline components. In Core 136-842B-2H, sediments immediately above and below the ash layers are indurated. The ash in Core 136-842B-3H is almost entirely altered to clay and phillipsite, but ash layers are recognizable as indurated layers of zeolitic clay. Radiolarians are present in minor amounts in Cores 136-842A-1H and 136-842B-1H; sponge spicules are common from Interval 136-842B-2H-1, 0 cm to 136-842B-2H-5, 78 cm. A section of yellowish brown nannofossil radiolarian ooze and clayey nannofossil ooze was recovered from Interval 136-842A-1H-6, 126–140 cm.

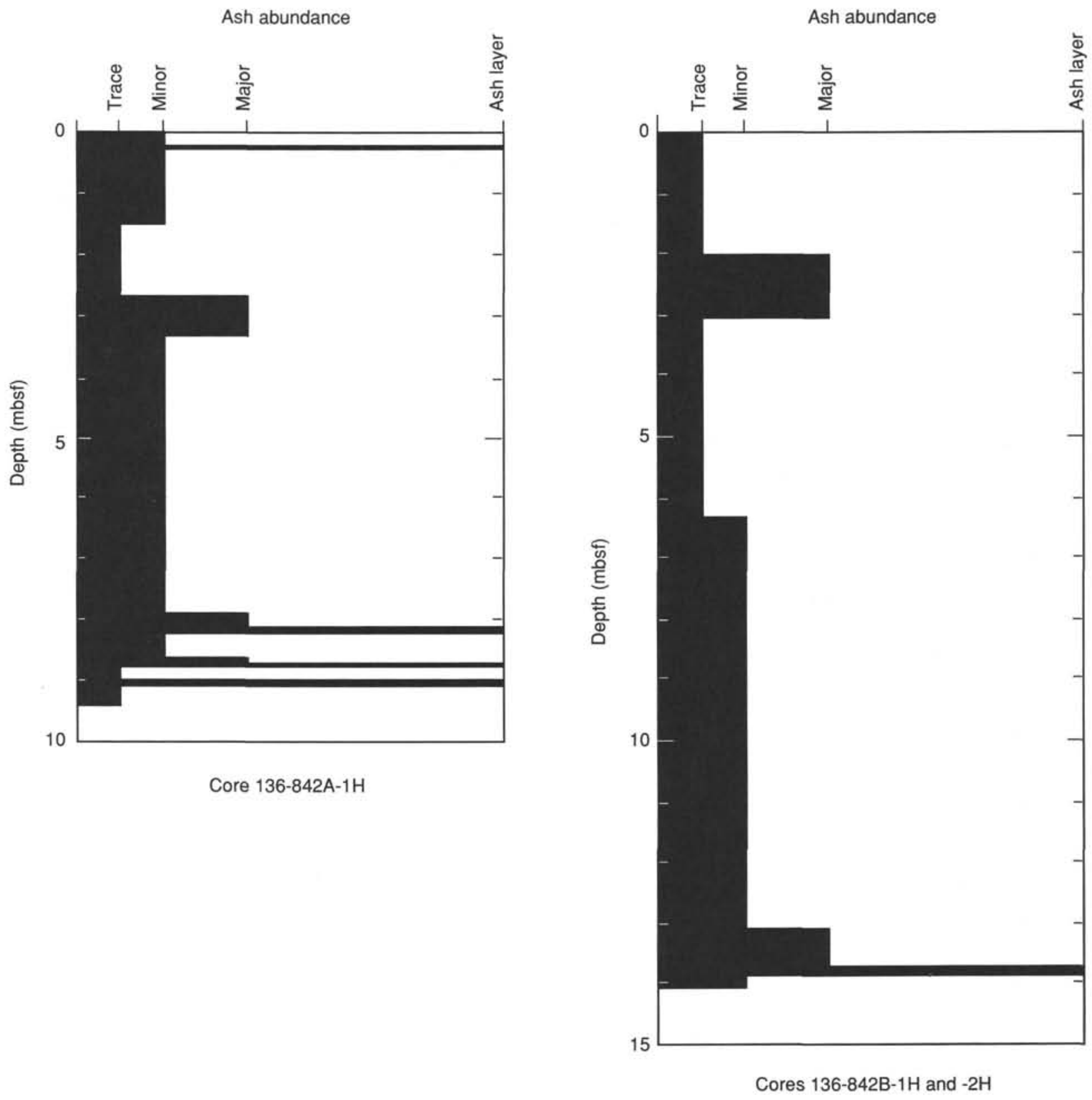

Figure 1. Location of ash layers and relative abundances of dispersed ash with depth in Cores 136-842A-1H, 136-842B-1H, and -2H.

Unit II (19.9–35.7 mbsf)

Lithologic Unit II consists of dark reddish brown clay and zeolitic clay and dark-brown to black claystone of late Eocene to middle Miocene age. The zeolites have been identified as phillipsite by X-ray diffraction analysis. The clays from Interval 136-842B-3H-3, 110 cm, to 136-842B-4H-4, 10 cm, are homogeneous and structureless with the exception of faint wavy laminations in Interval 136-842B-4H-1, 86–95 cm. From Interval 136-842B-4H-4, 10 cm, to 136-842B-4H-7, 61 cm, stringers of light brown clay, highly distorted by drilling disturbance, and indurated intervals are common. The stringers and indurated layers do not differ in composition from the surrounding brown clay as judged from smear-slide analysis. Nodules of dark-brown to black claystone are found in Interval 136-842B-4H-5, 74–115 cm, and throughout Core 136-842B-5H. X-ray diffraction analysis indicates that the claystones are cemented by opal-CT.

Unit III (35.7–237.7 mbsf)

Lithologic Unit III is represented by fragments of claystone and chert recovered in the core catchers of Cores 136-842B-6X to -10X (35.7–167.8 mbsf) and in Core 136-842C-1W (141.3–237.7 mbsf). The claystones are opal-CT-cemented, multicolored (dark gray, pale brown, and dark reddish brown), and generally homogeneous and structureless. In Section 136-842B-10X-CC (163.3 to 167.8 mbsf), pebbles and granules of claystone, glauconitic claystone, and opal-CT chert surround two chunks of yellowish red nannofossil ooze of Santonian age. Core 136-842B-10X was taken after drilling from 58.1 to 106.0 and from 115.7 to 163.3 mbsf, so the depths of these lithologies are not well constrained. A wash core from Hole 842C (Core 136-842C-1W) recovered fragments of gray, light greenish gray, dark red, and brown quartz cherts from a depth range of 141.3 to 237.7 mbsf. Some of the chert fragments have burrows filled with grayish orange pink chalk.

Occurrences of Volcanic Ash

The locations of discrete ash layers and the relative abundances of dispersed ash in Cores 136-842A-1H and 136-842B-1H and -2H are illustrated in Figure 1. Abundances of dispersed ash are taken from smear-slide descriptions. Ash layers recovered in Core 136-842A-1H have sharp basal contacts, fine upward, and grade into the overlying sediment (Fig. 2). Discrete layers of ash were not seen in Core 136-842B-1H. The ashes are composed primarily of glass, with minor amounts of plagioclase, augite, olivine, and Fe-Ti oxides (probably Ti-magnetites). The glass fragments are anhedral and do not have concave surfaces that would result from rapid degassing and explosion of a surface or near-surface magma.

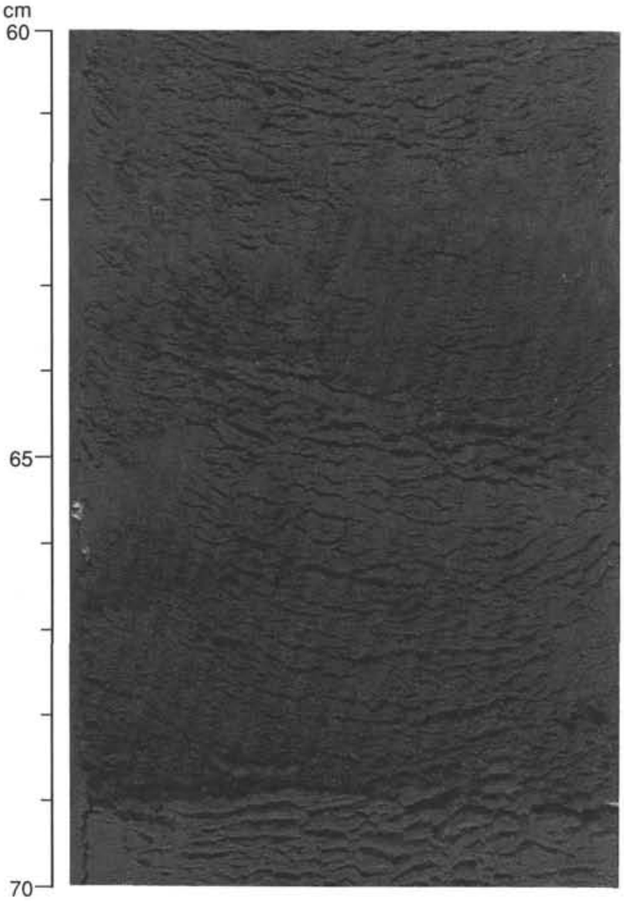

Figure 2. Photograph of ash layer in Section 136-842A-1H-6. The basal contact at 70 cm is sharp and horizontal. The ash fines upward to about 65 cm, above which there is a second fining upward sequence of ash.

BIOSTRATIGRAPHY

Calcareous Nannofossils

Sample 136-842A-1H-6, 130 cm, contains moderately to poorly preserved nannofossils, including *Calcidiscus macintyrei, Calcidiscus leptoporus, Pseudoemiliania lacunosa, Umbilicosphaera sibogae*, and *Gephyrocapsa* spp. Based on the co-occurrence of *C. macintyrei* and *Gephyrocapsa* spp., and the absence of discoasters, this sample is assigned to the Quaternary Zone NN19. Core-catcher samples from Cores 136-842A-1H and 136-842B-1H to -5H are barren of nannofossils.

Core 136-842B-10X contains less than 1 m of sediment, mostly gravel composed of chert and claystone fragments. It also contains several clumps of soft red clay with high concentrations of nannofossils. Samples 136-842B-10X-1, 12 cm, -10X-1, 19 cm, and -10X-CC, contain *Watzneuria barnesae, Prediscosphaera* spp., *Eprolithus floralis, Reinhardtites anthophorus,* and *Manivitella pemmatoidea.* With the absence of *Lucianorhabdus cayeuxii,* this assemblage indicates Zone CC15, of early Santonian age.

Radiolarians

Radiolarians extracted from Sample 136-842A-1H-CC include *Theocorythium trachelium, Lamprocyrtis neoheteroporos, Lithopera bacca, Euchitonia elegans, Euchitonia furcata, Hexacontium laevigatum, Axoprunum stauraxonium, Stylodictya validispina, Dictyocoryne truncatum, Dictyocoryne profunda, Anthocyrtidium* spp., and *Amphirhopalum ypsilon*. Based on the presence of *L. neoheteroporos* and *Anthocyrtidium angulare*. Sample 136-842A-1H-CC is assigned to the lower Quaternary *Anthocyrtidium angulare* Zone (sensu Sanfilippo et al., 1985). Sample 136-842A-1H-1, 28–30 cm, is assigned to the *Collosphaera tuberosa* Zone (lower upper Quaternary), based on the occurrence of the marker species *C. tuberosa*. Samples collected above this interval appear to lack *C. tuberosa*, but are assigned to the upper Quaternary on the basis of superposition. Other species present in Samples 136-842A-1H-1, 28–30 cm, and 136-842A-1H-2, 130–132 cm, include *Amphirhopalum ypsilon* (rare), *Lamprocyrtis nigrinae, Ommatartus tetrathalamus, Euchitonia elegans, Euchitonia fucata, Dictyocoryne truncatum, Dictyocoryne profunda, Spongaster tetras tetras, Liriospyris reticulata, Peripyramis circumtexta,* and *Lithopera bacca*. The uppermost zone of the Quaternary, the *Buccinosphaera invaginata* Zone, does not appear to be present in Hole 842A.

Sample 136-842B-1H-CC contains *Theocorythium trachelium, Dictyocoryne truncatum, Anthocyrtidium* sp., *Euchitonia furcata, Didymocyrtis tetrathalamus, Amphirhopalum ypsilon, Euchitonia elegans, Dictyocoryne profunda, and Lithopera bacca.* Based on the absence of the upper Quaternary species *Collosphaera tuberosa* and the lowermost Quaternary marker species *Anthocyrtidium angulare,* and the occurrence of *T. trachelium,* this sample is assigned to the lower Quaternary *Amphirhopalum ypsilon* Zone. *Lamprocyrtis neoheteroporos,* present in Sample 136-842A-1H-CC, has not been observed thus far in Hole 842B. Samples 136-842B-2H-CC, -3H-CC, -4H-CC, and -5H-CC are all barren of radiolarians.

Poorly preserved Upper Cretaceous radiolarians have been discovered in fragments of chert recovered in Core 136-842B-10X. Identifiable species include *Alievium murphyi* (Coniacian?; Santonian to Maestrichtian) and *Dictyomitra densicostata* (lower Cenomanian). Further investigation of radiolarian-bearing cherts will be conducted during post-cruise research.

Ichthyoliths

Cores 136-842B-3H and -4H contain primarily red clay. Samples 136-842B-3H-CC and -4H-CC contain common, well preserved ichthyoliths. Sample 136-842B-3H-CC contains Triangle with triangular projection, Narrow triangle cross-hatchured, Triangle with base angle, Flexed triangle shallow inbase >120 degrees, Flexed triangle, Short triangle stepped margin, Narrow triangle ragged base and Long triangle stepped margin. The co-occurence of these forms suggests an age of middle to early late Miocene, although according to Doyle and Riedel (1985), the top of Narrow triangle cross-hatchured occurs lower than most ichthyoliths in Sample 136-842B-3H-CC. Its occurrence with stratigraphically higher forms may be accounted for by reworking at or near the base of the core. Sample 136-842B-4H-CC contains Triangle-pointed margin ends, Triangle with base angle, triangle medium wing,

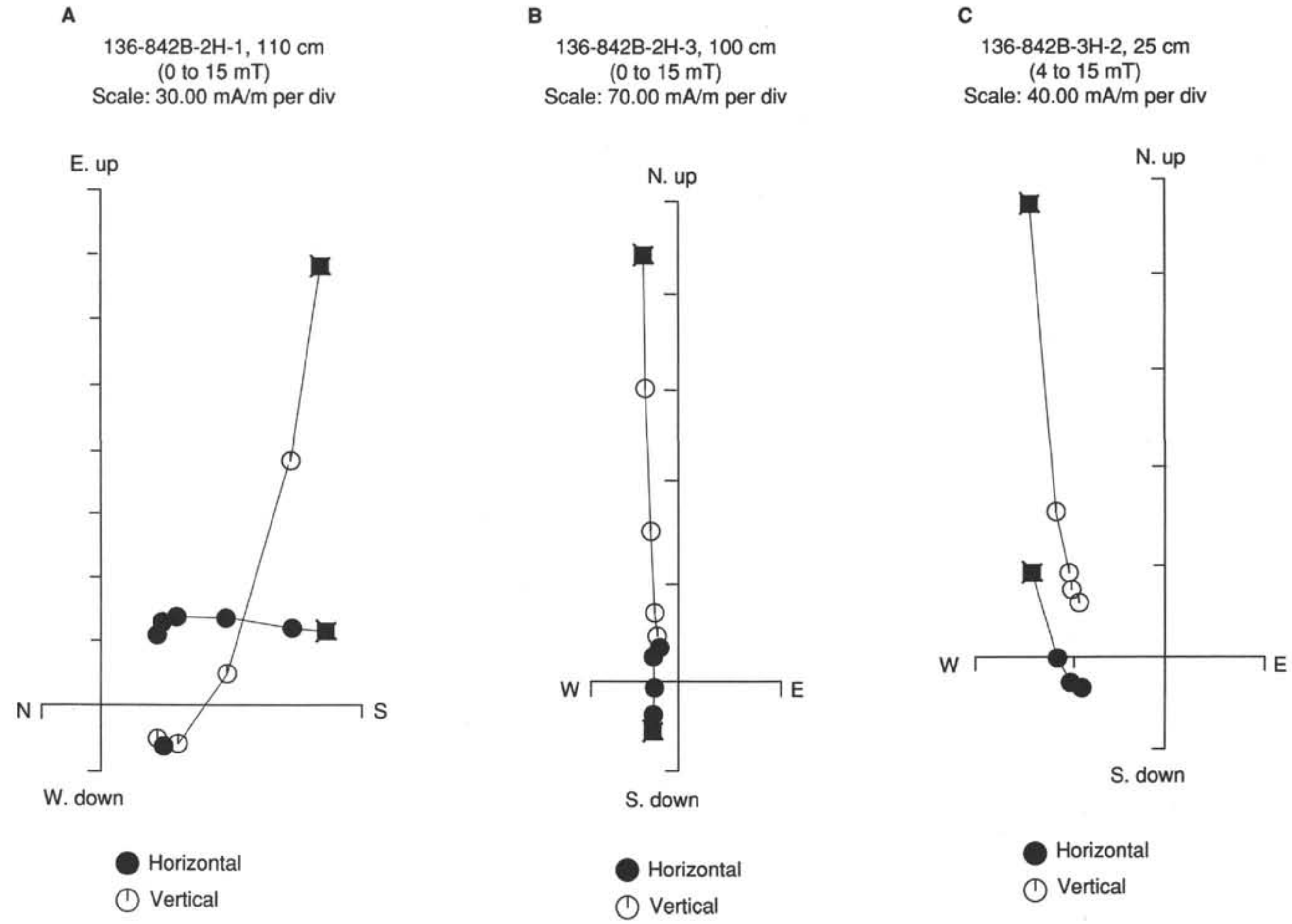

Figure 3. Orthogonal plots of AF demagnetization data at three depths in the archive cores from Hole 842B. **A.** Normal polarity inferred from downward inclination of higher coercivity component in Interval 136-842B-2H-1, 110 cm; **B.** Reversed polarity inferred from upward inclination in 136-842B-2H-3, 100 cm. In **A** and **B**, coordinates are relative to the fiducial line on the core. **C.** Illustrates the problematical remanence in oriented Interval 136-842B-3H-2, 25 cm; we have not been able to determine this polarity record on board ship but, as this illustration shows, it may be possible to do so with further work.

Narrow triangle cross-hatchured, which indicate an age of late Eocene to middle Miocene. Two other forms, Triangle with high inline apex and Skewed four or five peaks, may indicate a more restricted age range of early Oligocene to early Miocene (Doyle and Riedel, 1979; 1985). The identification of these two forms, however, remains uncertain until further shore-based study is complete.

PALEOMAGNETISM

The principal shipboard paleomagnetic measurements at Site 842 consisted of scans of the archive-half of the core from Hole 842A (Core 136-842A-1H, 0–9.5 mbsf) and Cores 136-842B-1H through -4H of Hole 842B (0-34.8 mbsf) using the ODP cryogenic magnetometer. Measurements were made of total natural remanent magnetization (NRM) and of the remanence retained after alternating field (AF) demagnetization[3] at 2, 4, 7, and 10 mT at 5-cm intervals on all these cores.

Demagnetization at 12- and 15-mT steps were performed on Cores 136-842B-2H and -3H in an attempt to further clarify the original magnetic signature that might reside beneath the large drilling-related overprint observed in the NRM of these cores. Typical results from the demagnetization experiments are illustrated in Figure 3.

The general features of the observed remanence in the above cores are:

1. The initial NRM is typically 100 to 400 mA/m and is directed steeply upward. This magnetization is shown in the NRM plots given in Figures 4 to 9. We believe the NRM to be dominated by a drilling-related secondary component (see later discussion) as has been found on previous ODP legs.
2. Progressive AF demagnetization to 10 or 15 mT (Figs. 10–15) removes much but not all of this drilling-induced spurious component. This level of demagnetization is sufficient to reveal the polarity of the underlying stable component in Cores 136-842A-1H, 136-842B-1H and -2H, but in most cases does not isolate the stable component. For Cores 136-842B-3H-3 and -4, demagnetization levels of 15 mT were insufficient to reveal even the general magnetic polarity pattern. As a result, the shipboard measurements are good for polarity stratigraphy at depths above 15.8 mbsf, but the measurements should not be used for interpretations requiring a precise knowledge of the stable magnetization direction.

APC Core 136-842B-5H was not measured, because it is highly disturbed. The XCB cores from deeper in Hole 842B and the wash-core from Hole 842C were not sampled because their fragmentary

[3]Demagnetization was 5 mT instead of 4 mT on Section 136-842A-1H-1.

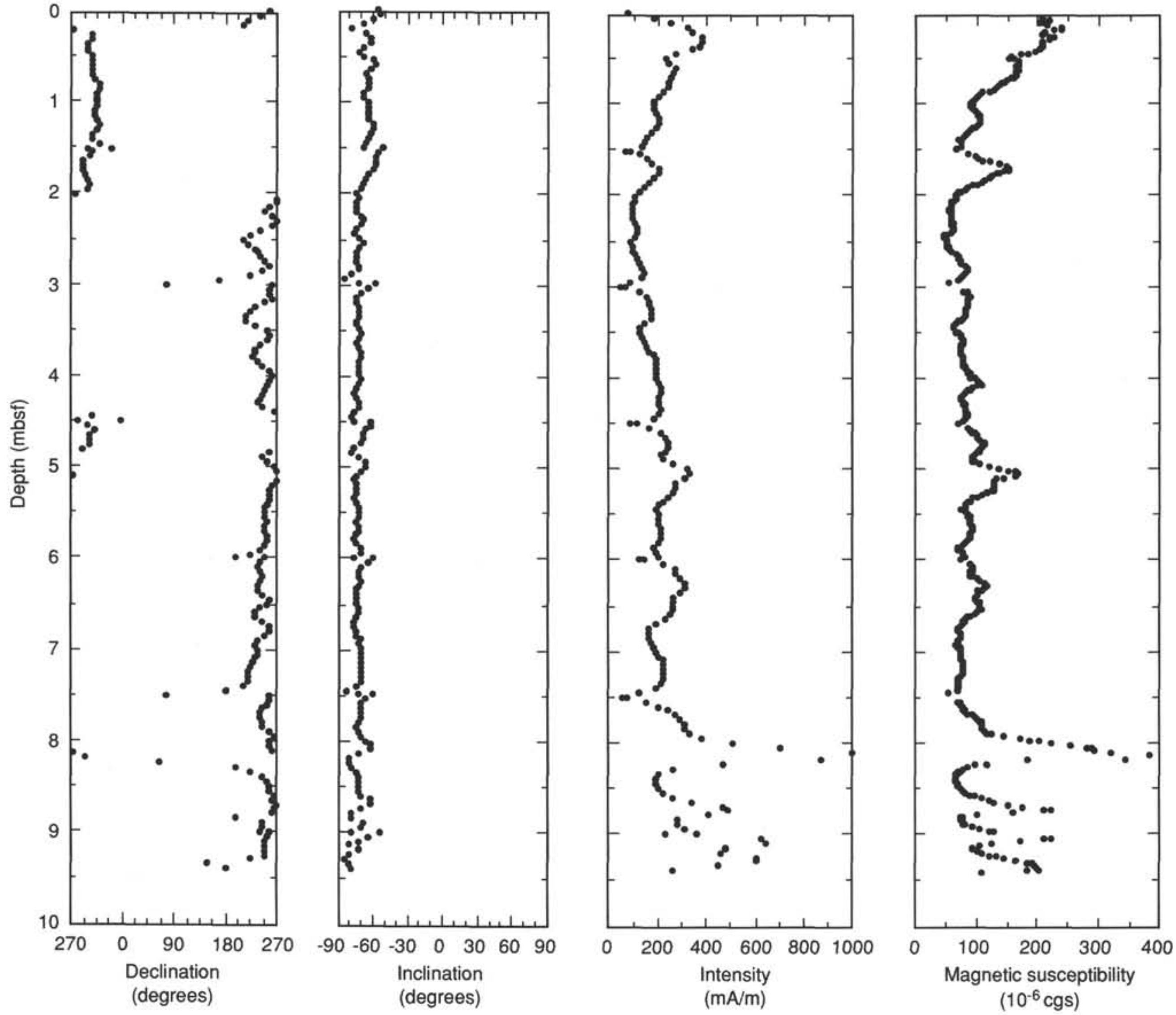

Figure 4. Plots of total NRM and initial susceptibility vs. depth (mbsf) in Core 136-842A-1H. Declination has been inferred from the discovered polarity sequence.

recovery of broken pieces precluded any useful paleomagnetic information being present.

All the APC cores were logged for initial magnetic susceptibility and the results are compared with the remanent magnetization in Figures 4–9.

Polarity Stratigraphy

Cores 136-842A-1H and 136-842B-1H both display several clear polarity zones (Figs. 10 and 11). Both cores have an N/R (i.e., normal overlying reverse) polarity transition at about 2 mbsf and R/N and N/R transitions at about 4 m and 4.75 m, respectively. The polarity record continues in the lower portion of Core 136-842B-2H with a R/N transition at Interval 136-842B-2H-2, 120 cm, an N/R transition at Interval 136-842B-2H-3, 80 cm, a R/N transition at 125 cm in the same section, an N/R transition at Interval 136-842B-2H-4, 65 cm and a R/N transition at 145 cm in this section. Core 136-842B-2H ends in a normal polarity interval (Fig. 12). This record is sufficiently clear that we have been able to use the paleomagnetics to orientate the cores, and Figures 4–6 and 9–11 are all plotted on this reoriented basis rather than relative to the unknown azimuth of the fiducial mark on these cores.

Our preferred interpretation is that the transitions at about 2 m, 4 m, and 4.75 m represent the Matuyama-Brunhes transition and the Jaramillo event, respectively. The polarity interval sequence in the lower part of Core 136-842B-2H is very reminiscent of the Gauss magnetic epoch with the Kaena and Mammoth events within it.

On the assumption of fairly constant sedimentation rates, we would expect to find the Olduvai normal event between about 6 and 8 m in both holes. Core 136-842A-1H is reversely magnetized from 4.9 mbsf to its base at 9.5 mbsf with no evidence of any normal polarity zone. Core 136-842B-1H is reversed near its base at 6.3 mbsf; the top 70 cm of the next core is disturbed both mechanically and in its remanence. The susceptibility records observed throughout the cores from the two holes are in close agreement (Figs. 4–6) except for the disturbed zone at the top of Core 136-842B-2H. Immediately beneath the disturbed zone within Core 136-842B-2H there is a hint of normal polarity in a sequence of three normal and six transitional readings over the 40 cm immediately below the disturbed zone. If this were accepted as evidence of a normal interval, then a mismatch between the two holes only 10 m apart is implied.

Below Core 136-842B-2H the polarity record is less clear (Figs. 13 and 14). Although the top of Core 136-842B-3H appears to be

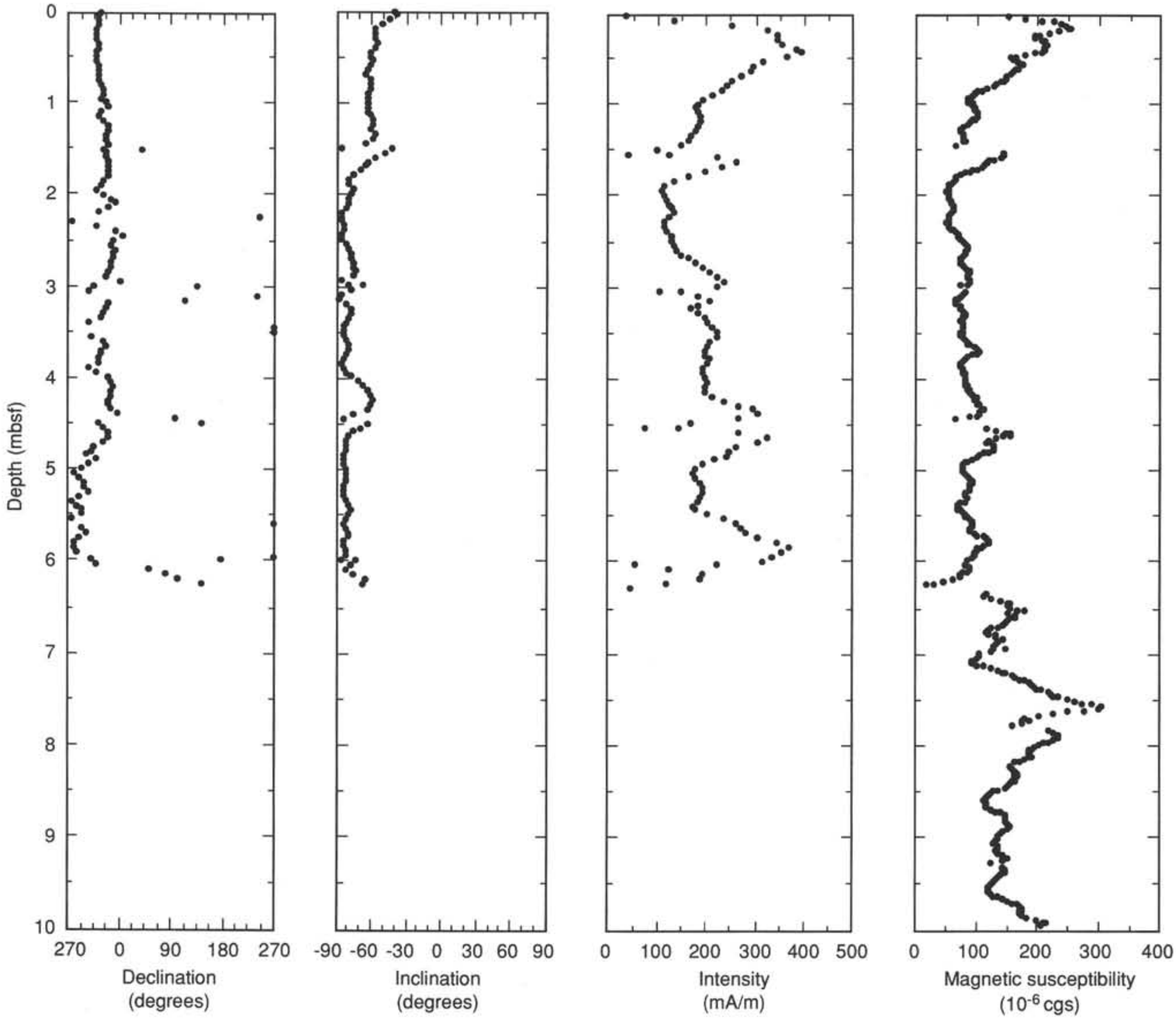

Figure 5. Plots of total NRM and initial susceptibility vs. depth (mbsf) in Core 136-842B-1H. Declination has been inferred from the discovered polarity sequence.

reversely magnetized, it is somewhat disturbed and it is possible that the base of the Gauss is obscured within the upper part of this core. Intensity is lower from this level downward, and the spurious component appears to be magnetically harder, so we are not confident of having identified primary polarity (see Fig. 3C) except over limited intervals, and will have to investigate this further.

Sedimentation Rates

In our currently preferred model (Figs. 15 and 16), the Brunhes is relatively thin compared with the underlying upper Matuyama interval. If the whole of the Brunhes is assumed to be present then the average sedimentation rate was about 2.5 mm/k.y.; this low rate may be due to hiatuses at the top or within the Brunhes section. The Matuyama section down to the base of the Jaramillo corresponds to an average of 11.6 mm/k.y., and on this basis the duration of the Jaramillo would be estimated as 50 k.y., which is consistent with estimates in recent syntheses (Berggren et al., 1985).

Assuming that the lowest polarity intervals in Core 136-842B-2H are indeed the Gauss, the average sedimentation rates for the lower Matuyama and Gauss are 3.3 and 4.8 mm/k.y. respectively (although of course we do not know the amount or timing of variation in these rates). Again, estimates of the duration of the reversed intervals within the Gauss, based on these average rates, are consistent with the geomagnetic polarity time scale. The apparently low sedimentation rate in the lower Matuyama relative to the units above and below may be due to one or more hiatuses that must be present to account for the missing Olduvai record.

Susceptibility and Intensity

NRM intensity is typically 100 to 400 mA/m, and is reduced to 25% or less in an alternating field of 10 mT. These are unusual properties for deep-sea sediments and probably signify the imposition of IRM in a strong magnetic field (see next section). Intensity is also enhanced in mechanically disturbed sediment in Cores 136-842B-2H, -3H and -4H.

Initial susceptibility ranges from about 50–250 $\times 10^{-6}$ (SI). In Hole 842A and the upper 15 m of Hole 842B, susceptibility, total and 10 mT demagnetized intensity correlate well with each other and between holes. All are probably correlated with ash content in the sediment. Below 15 m intensity and susceptibility do not correlate

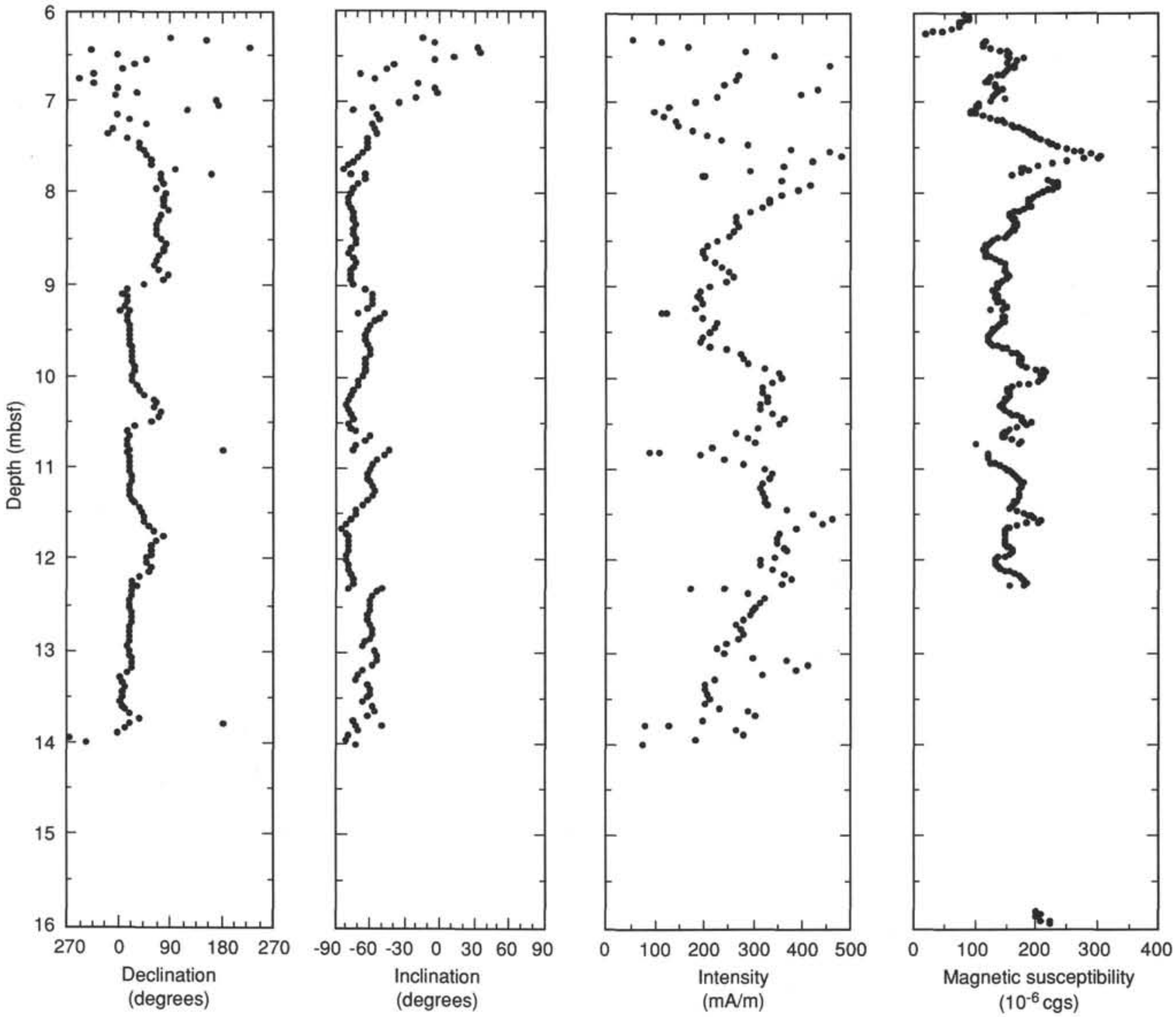

Figure 6. Plots of total NRM and initial susceptibility vs. depth (mbsf) in Core 136-842B-2H. Declination has been inferred from the discovered polarity sequence.

consistently, though both are enhanced in the disturbed top of Core 136-842B-3H.

There are also prominent effects on our measurements at the ends of core sections and we have not determined whether these are entirely geometric effects in the magnetometer or whether disturbance during core sectioning contributes.

Finally, there is the tantalizing observation of fluctuations in intensity with wavelength of about 0.5 m in all the cores that carry a paleomagnetic signal. It will be interesting to determine whether there is a geomagnetic cause of these fluctuations or whether they are fully accounted for by the several effects mentioned above.

Drilling-related Magnetization

All cores measured on Leg 136 had a strong secondary component oriented upcore at a steep angle of about 70°. In many cases this secondary component totally obscures the stable moment in the NRM. It is observed in minicubes taken from the center of the core as well as in half-core measurements on both the archive and working halves of the core using the ODP cryogenic magnetometer. Because the direction of the secondary moment is steeply "uphole" it is very likely acquired during drilling or passage through the drill pipe, as has been suggested by previous workers. However, our observation that it also has a systematic declination relative to the archive-half core is unexpected, for one would expect variations in the orientation of the core to produce variations in the direction of the imposed magnetization.

We measured the total NRM of working halves of several core sections and found that declination was still approximately north in magnetometer coordinates. Thus when corrected for the 180°degree rotation of the working half the declinations in the two halves were approximately 180° different. This implies either that the declination of the spurious component is different in the two halves of the core or that the difference is due to the measurement process itself. We suspect the latter because the only asymmetry in the process is in the displacement of the half-cores from the axis of the magnetometer sensor system. This will be tested using U-channel samples in various positions in the magnetometer.

Sampling for Shore-based Study

All APC cores were sampled for subsequent work. This sampling included (1) standard cube samples at about 20-cm intervals to verify

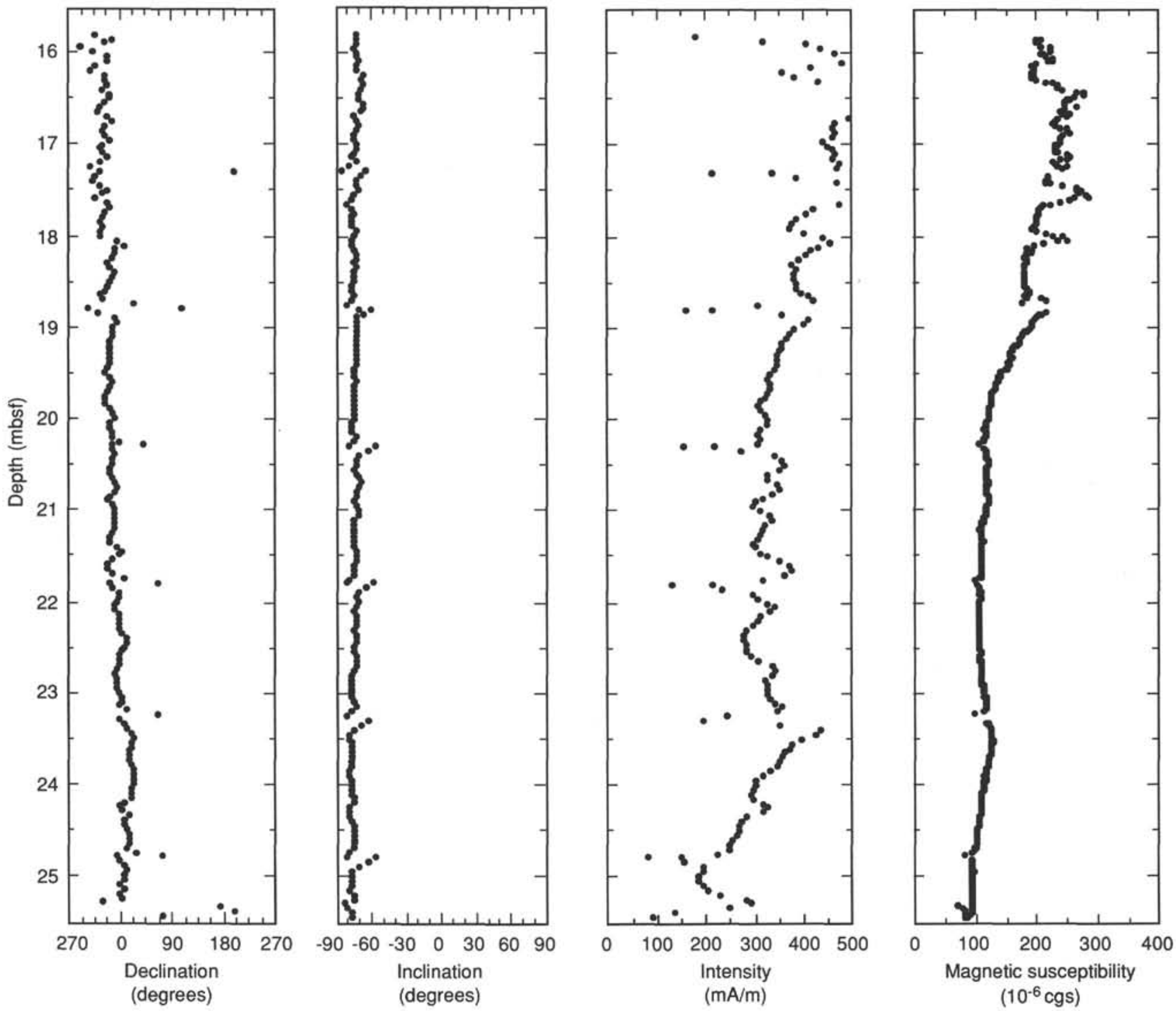

Figure 7. Plots of total NRM and initial susceptibility vs. depth (mbsf) in Core 136-842B-3H. Declination was derived from downhole orientation.

and refine the polarity stratigraphy described above and (2) continuous sequences of 1-cm^3 cores across the identified polarity inversions, extending about 25 cm above and below, to study the details of the transition zones.

Preliminary Shore-based Laboratory Measurements

Initial shore-based laboratory measurements at Oxford University (W. Scott, pers. comm., 1991) confirm the dominance of the steep upward soft component of NRM. Intensities measured in the laboratory seem to be lower than shipboard calculations; we have yet to determine whether this signifies decay in the few months since sampling or is a calibration difference to be resolved.

As with the shipboard measurements, the inclination of NRM is lower in the depth ranges that are shown to be of normal polarity by shipboard AF demagnetization. In the Oxford University laboratory we routinely calculate confidence limits (α_{95}) on *individual* remanence directions. An intriguing feature of Leg 136 samples is that α_{95} is substantially higher (typically 7°) where inclination is low; where inclination is high, $\alpha_{95} \approx 1°–2°$ as is found in most rocks.

INORGANIC GEOCHEMISTRY

Introduction

The shipboard inorganic geochemistry procedures at Site 842 consisted of (1) chemical analyses of interstitial water (see Table 3), (2) collection of samples for shore-based trace element analysis, and (3) X-ray diffraction (XRD) analysis of the corresponding squeeze cakes. Details of the shipboard analytical procedures have been described in the explanatory notes (see Explanatory Notes, this volume). Because all samples were collected from unconsolidated pelagic red clay sediments, 5-cm long whole-round cores were squeezed; interstitial water recoveries were excellent with volumes ranging from 30 to 65 ml. Two whole round samples were taken from the first core of Hole 842A and from each of the first four cores from Hole 842B; no samples were taken from Core 136-842B-5H because

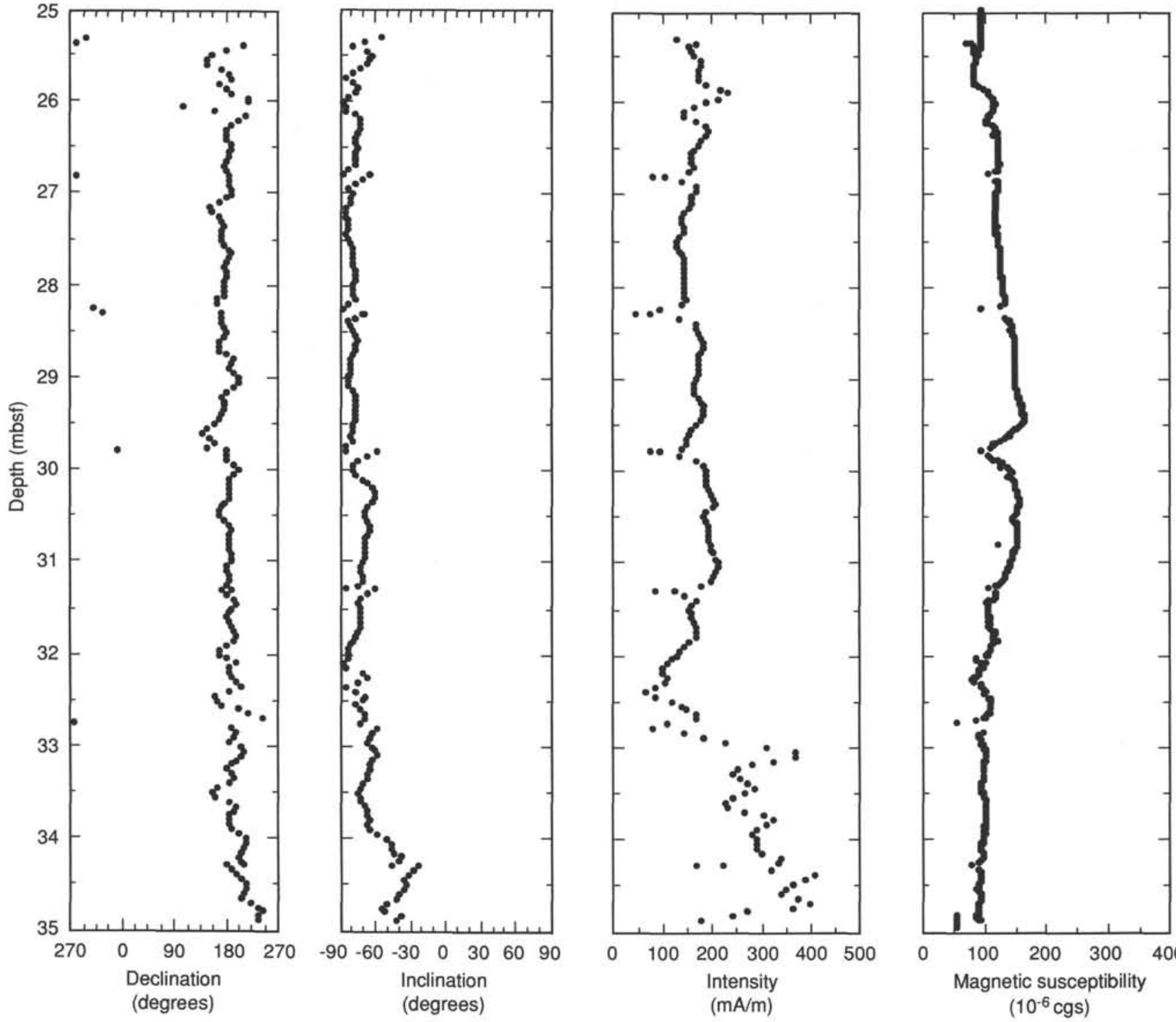

Figure 8. Plots of total NRM and initial susceptibility vs. depth (mbsf) in Core 136-842B-4H. Declination was derived from downhole orientation.

only a 90-cm section was recovered. Subsequent coring attempts recovered chert or silicified clay fragments, or were unsuccessful, and no further sediments suitable for interstitial water recovery were obtained at Site 842.

Concentration gradients at Site 842 are generally weak as would be expected from the very slow deposition rate of pelagic clays, thereby allowing a large extent of diffusional equilibration. Furthermore, interstitial water samples collected from Site 842 represent only the first 34 mbsf over which sedimentary reactions have occurred to a limited extent for most constituents. Only NH_4^+, NO_3^-, PO_4^{3-}, and silica exhibit relatively large variations in concentration as a function of depth downhole and attest to the occurrence of a limited extent of sedimentary diagenetic reactions.

Salinity and Chloride

The salinity of Site 842 interstitial water decreases slightly from a value of 35‰ at the top of Hole 842A to approximately 34‰ near 28mbsf. A slight increase to 34.5‰ in Sample 136-842B-4H-5, 145–150 cm, may be due to some contamination with drill water. This suspicion arises from our observation of core disturbance in this interval and is partially supported by slightly greater Cl^- and SO_4^{2-} concentrations. However, concentrations of other constituents do not support this hypothesis. Overall salinity and Cl^- remain within approximately 1% of normal seawater values.

Alkalinity and pH

Alkalinity generally decreases from a near seawater value at the top of the sediments of Site 842 to near 1.3 meq/L at 32.75 mbsf. A general decrease in alkalinity is common in oceanic sediments poor in organic matter (Gieskes, 1981). Interstitial water pH exhibits no significant trend and ranges from 7.41 to 7.80.

Sulfate

The degradation of organic matter appears to be a minor process in the sediments of Site 842 as evidenced by less than 10% depletion of SO_4^{2-} at 28.25 mbsf, or evidence of SO_4^{2-} depletion has been largely erased by diffusion. Nonetheless, a general decrease in SO_4^{2-} is observed downhole, and suggests that organic matter degradation is

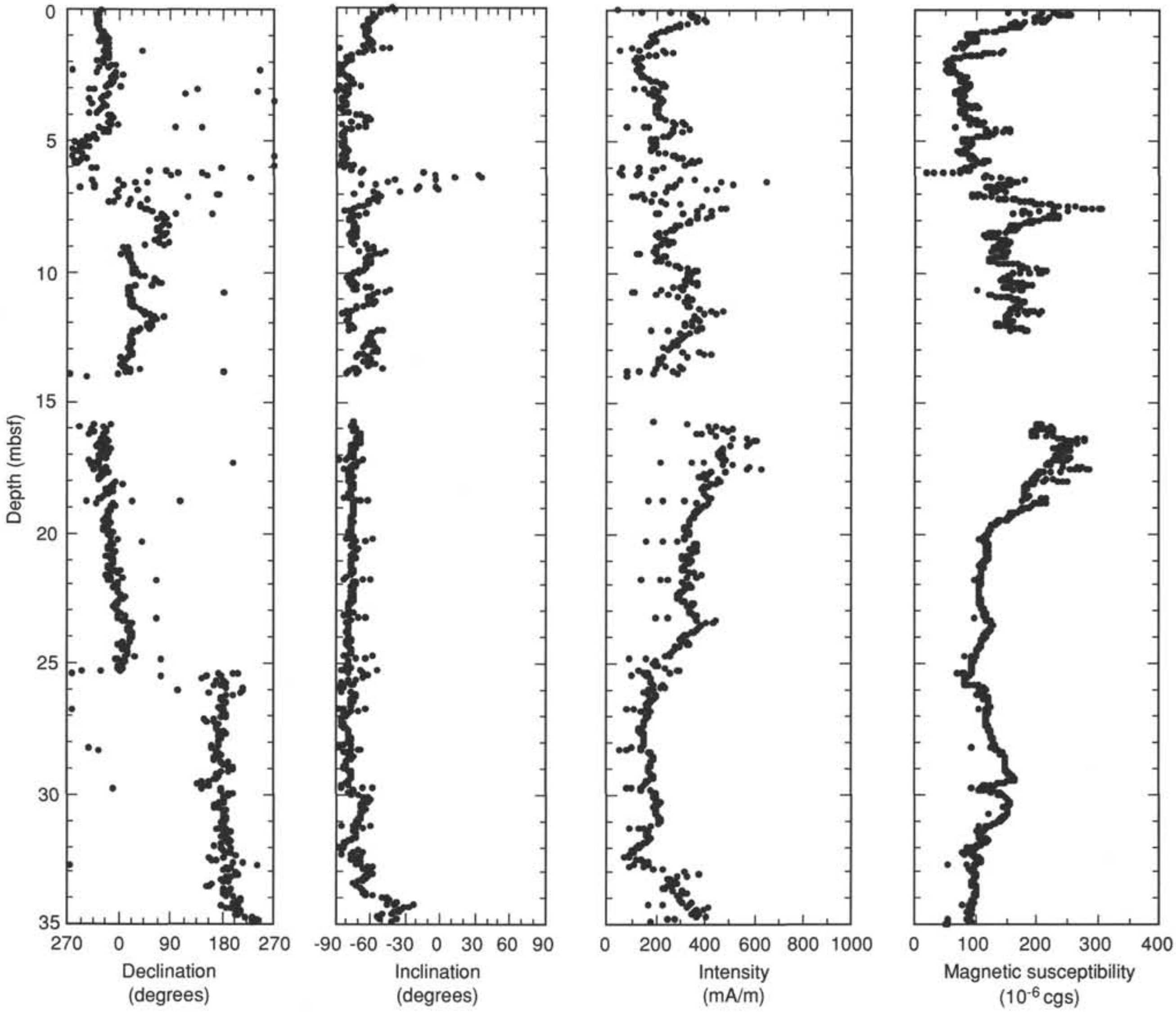

Figure 9. Plots of total NRM and initial susceptibility vs. depth (mbsf) in Hole 136-842B; composite of Figures 5 to 8.

Table 3. Composition of interstitial water.

Core Section interval (cm)	Depth (mbsf)	pH	Alk. (mM)	Sal. (g/kg)	Cl^- (mM)	Mg^{2+} (mM)	Ca^{2+} (mM)	SO_4 (mM)	PO_4^{3-} (μM)	NH_4^+ (μM)	Si (μM)	K^+ (mM)	NO_3^- (μM)
136-842A-													
1H-2, 145–150	2.95	7.70	2.290	35.0	550.6	54.2	10.5	27.4	2.16	13.5	319	11.3	48.5
1H-5, 145–150	7.45	7.71	2.360	35.0	557.3	53.1	10.4	28.0	1.95	7.6	306	11.8	21.6
136-842B-													
1H-1, 145–150	1.45	7.80	2.490	34.8	554.3	53.0	10.2	27.7	2.57	16.4	323	11.4	20.6
1H-3, 145–150	4.45	7.44	2.320	35.0	558.4	52.7	10.4	28.4	1.74	18.5	348	11.8	27.6
2H-3, 145–150	10.45			34.8	562.6	51.4	10.5	27.9	0.92	21.5	175	11.7	51.9
2H-5, 145–150	13.45	7.65	1.806	34.0	554.3	49.8	10.3	28.5	0.95	19.3	193	12.5	28.5
3H-2, 145–150	18.75	7.41		34.0	556.6	48.9	11.0	27.2	0.50	42.7	160	11.3	29.6
3H-5, 145–150	23.25	7.57	1.530	34.0	548.3	50.7	11.9	26.8	0.71	23.7	263	12.0	24.3
4H-2, 145–150	28.25	7.56	1.373	33.8	561.9	51.3	12.4	26.5	0.92	77.8	433	11.7	21.3
4H-5, 145–150	32.75	7.57	1.323	34.5	564.4	50.5	12.7	27.8	1.12	150.4	649	12.8	22.2

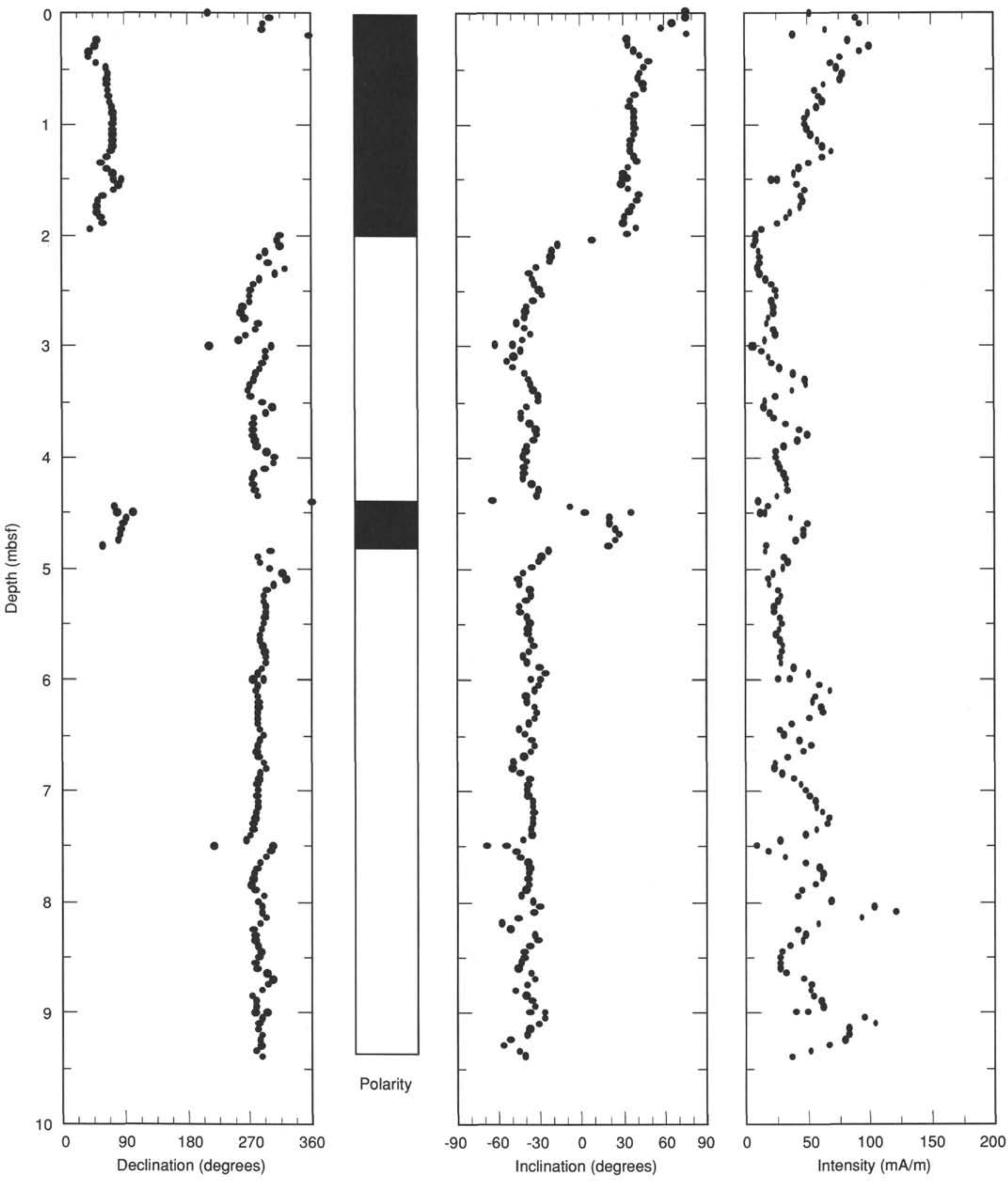

Figure 10. Plots of remanent magnetization (after AF demagnetization to 10 mT) vs. depth (mbsf) in Core 136-842A-1H. Declination has been inferred from the discovered polarity sequence. Polarity is shown as black for normal, white for reversed.

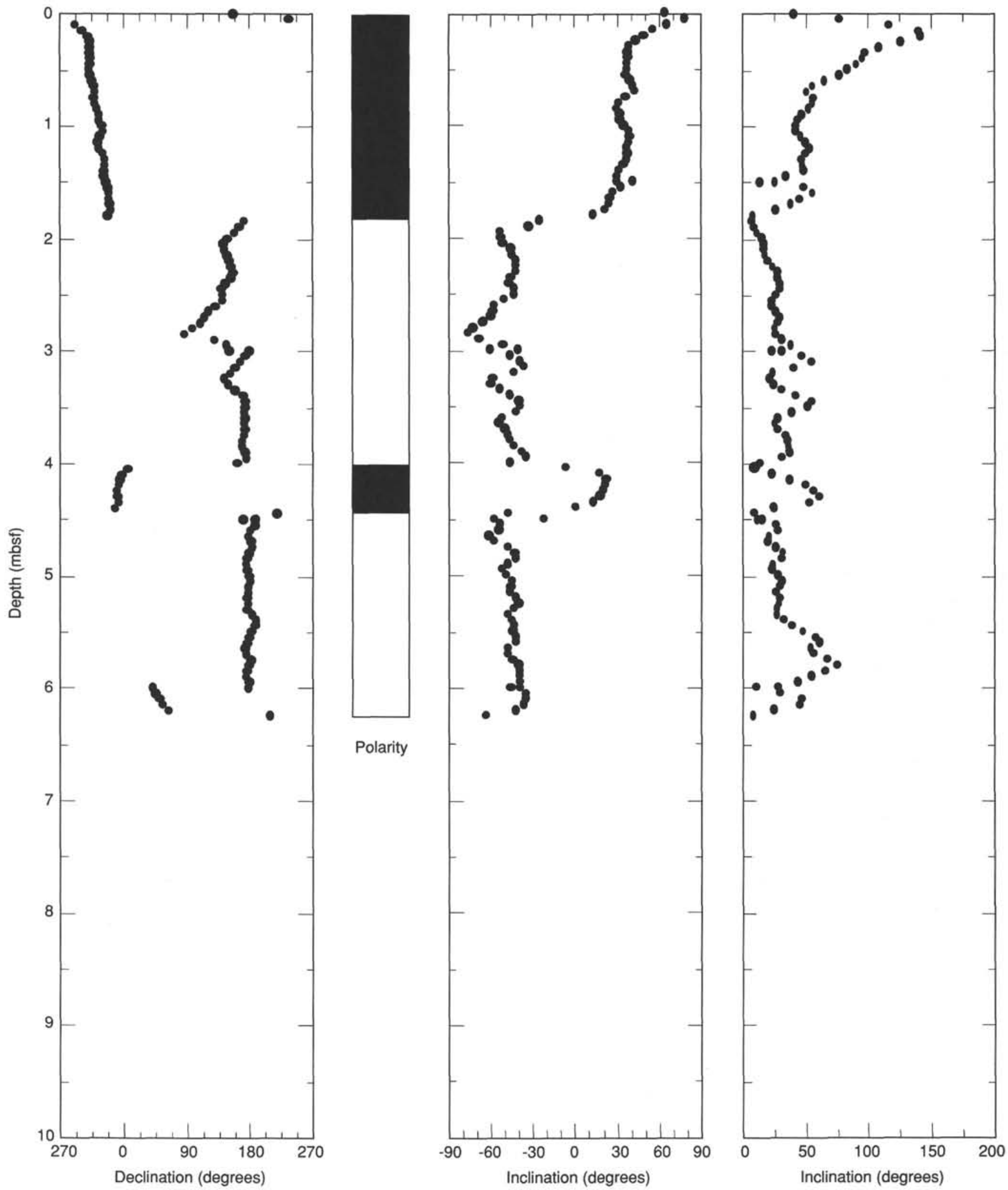

Figure 11. Plots of remanent magnetization (after AF demagnetization to 10 mT) vs. depth (mbsf) in Core 136-842B-1H. Declination has been inferred from the discovered polarity sequence. Polarity is shown as black for normal, white for reversed.

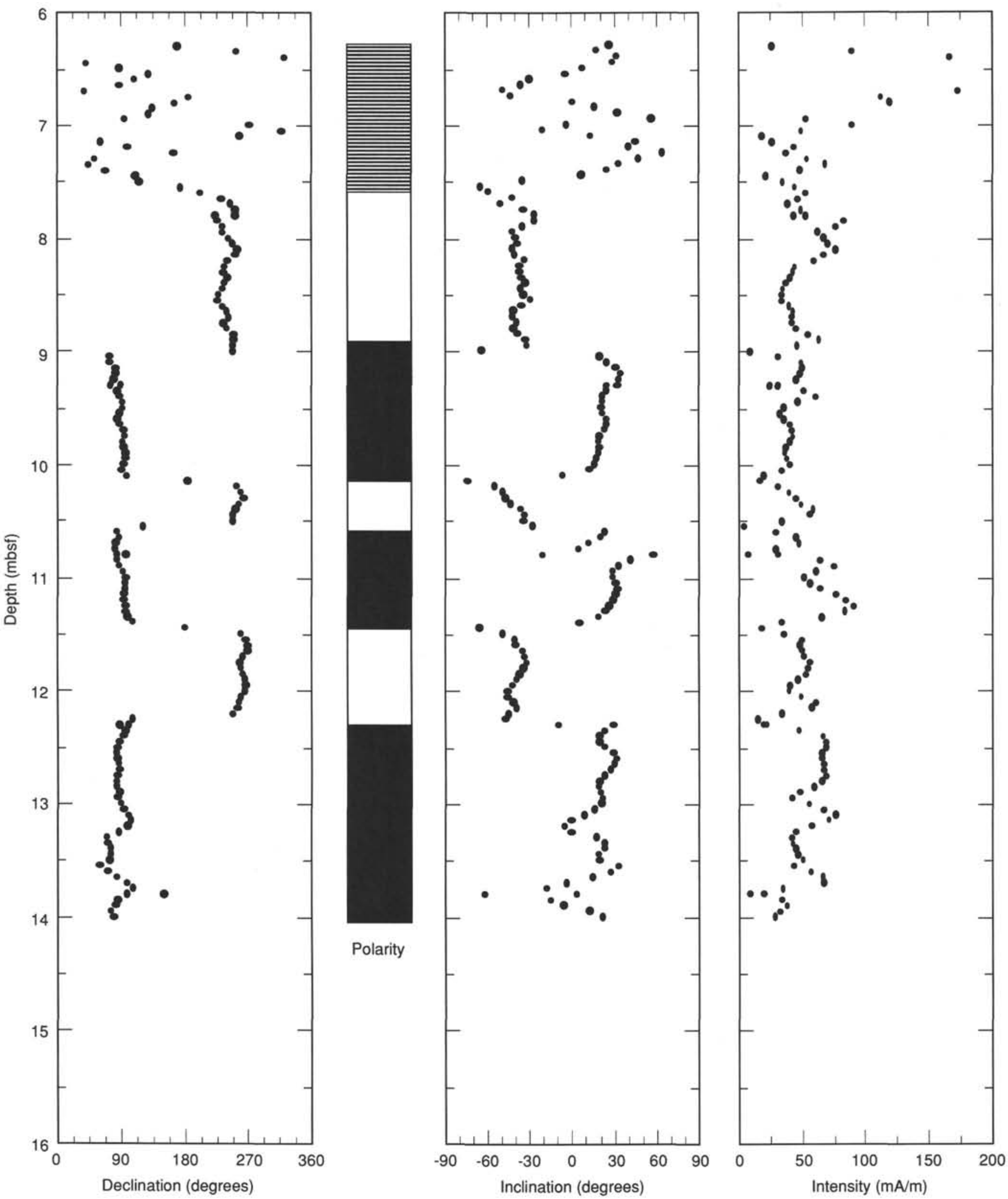

Figure 12. Plots of remanent magnetization (after AF demagnetization to 10 mT) vs. depth (mbsf) in Core 136-842B-2H. Declination has been inferred from the discovered polarity sequence. Polarity is shown as black for normal, white for reversed; horizontal lines indicate the disturbed interval.

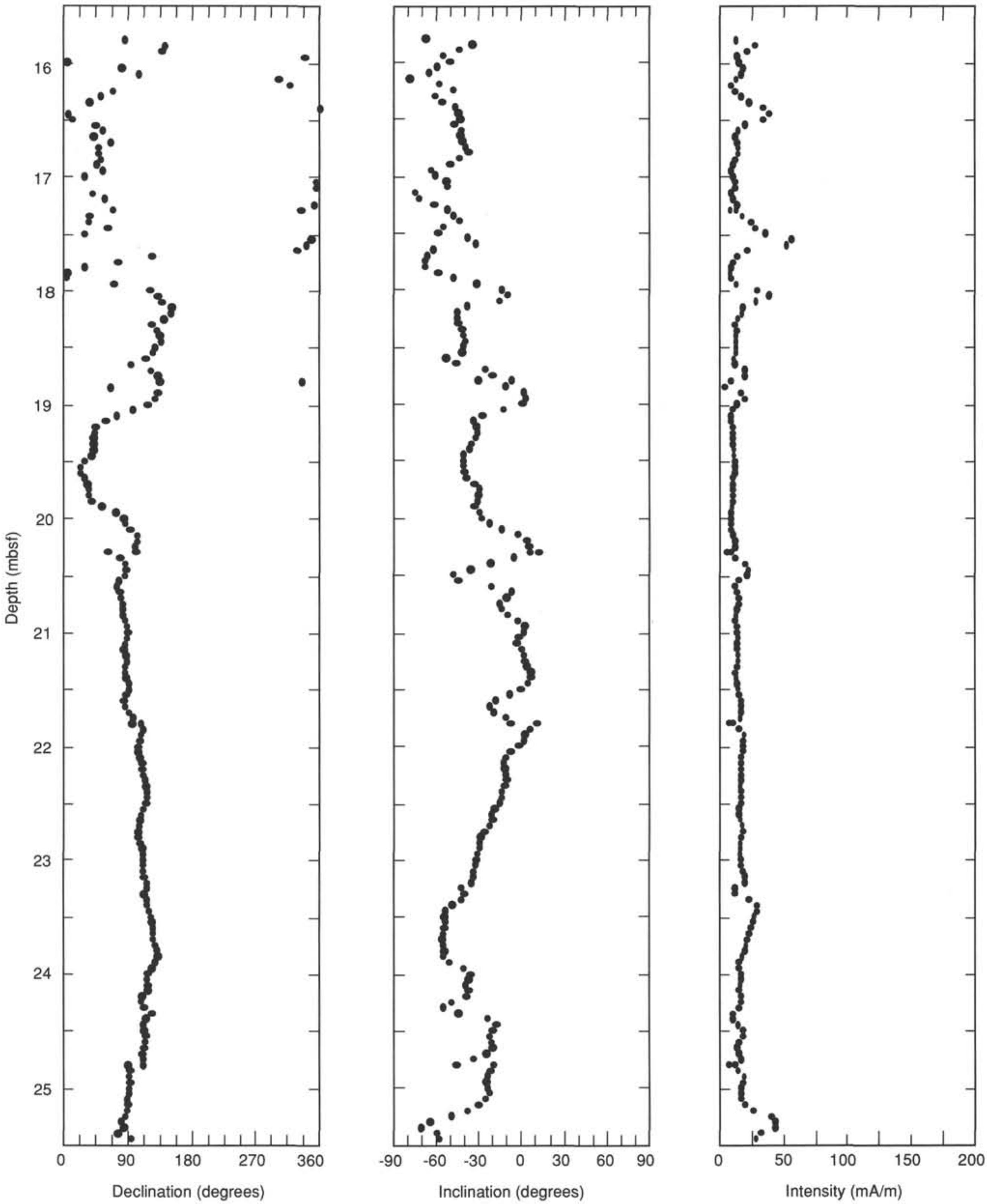

Figure 13. Plots of remanent magnetization (after AF demagnetization to 10 mT) vs. depth (mbsf) in Core 136-842B-3H. Declination was derived from downhole orientation.

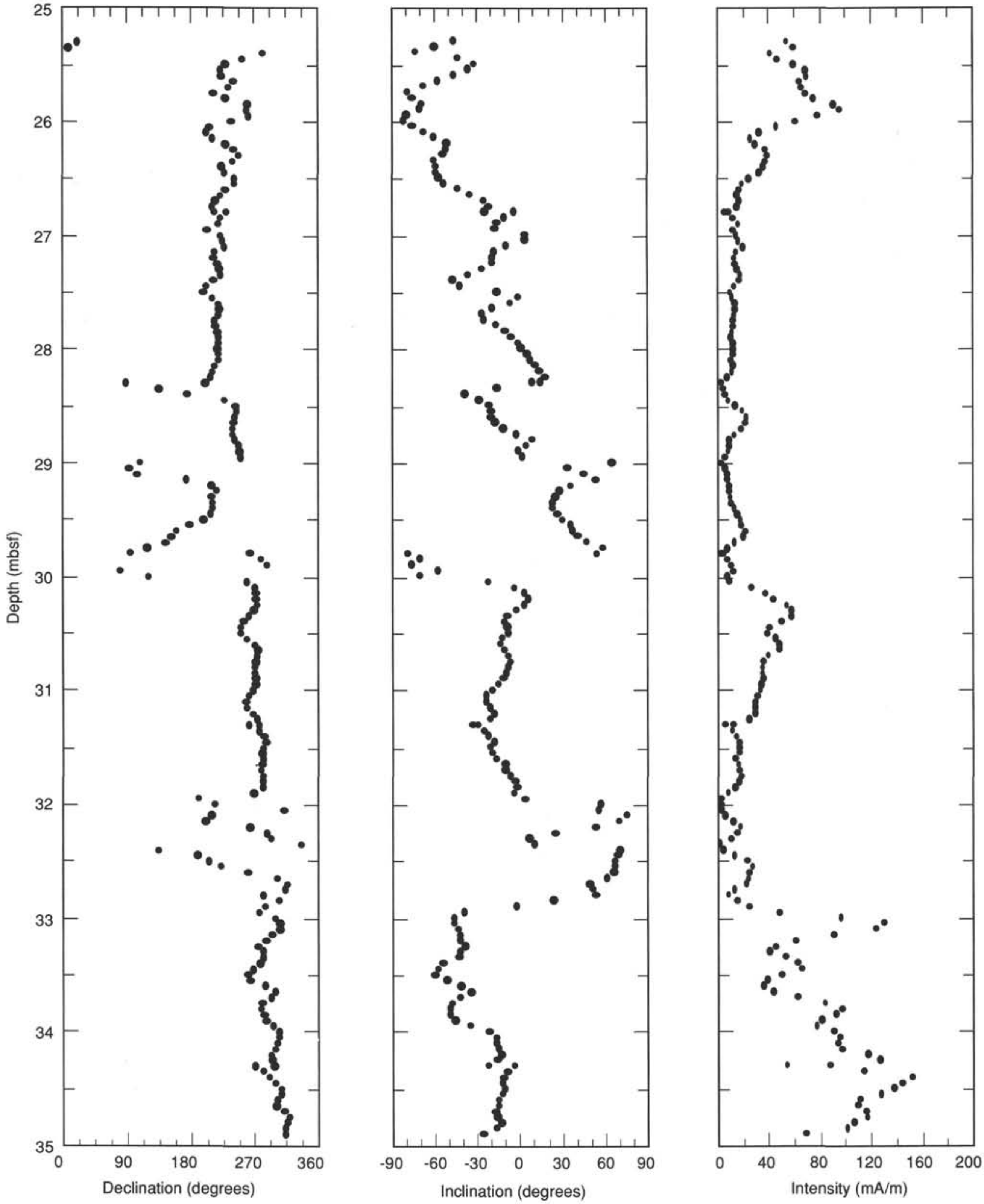

Figure 14. Plots of remanent magnetization (after AF demagnetization to 10 mT) vs. depth (mbsf) in Core 136-842B-4H. Declination was derived from downhole orientation.

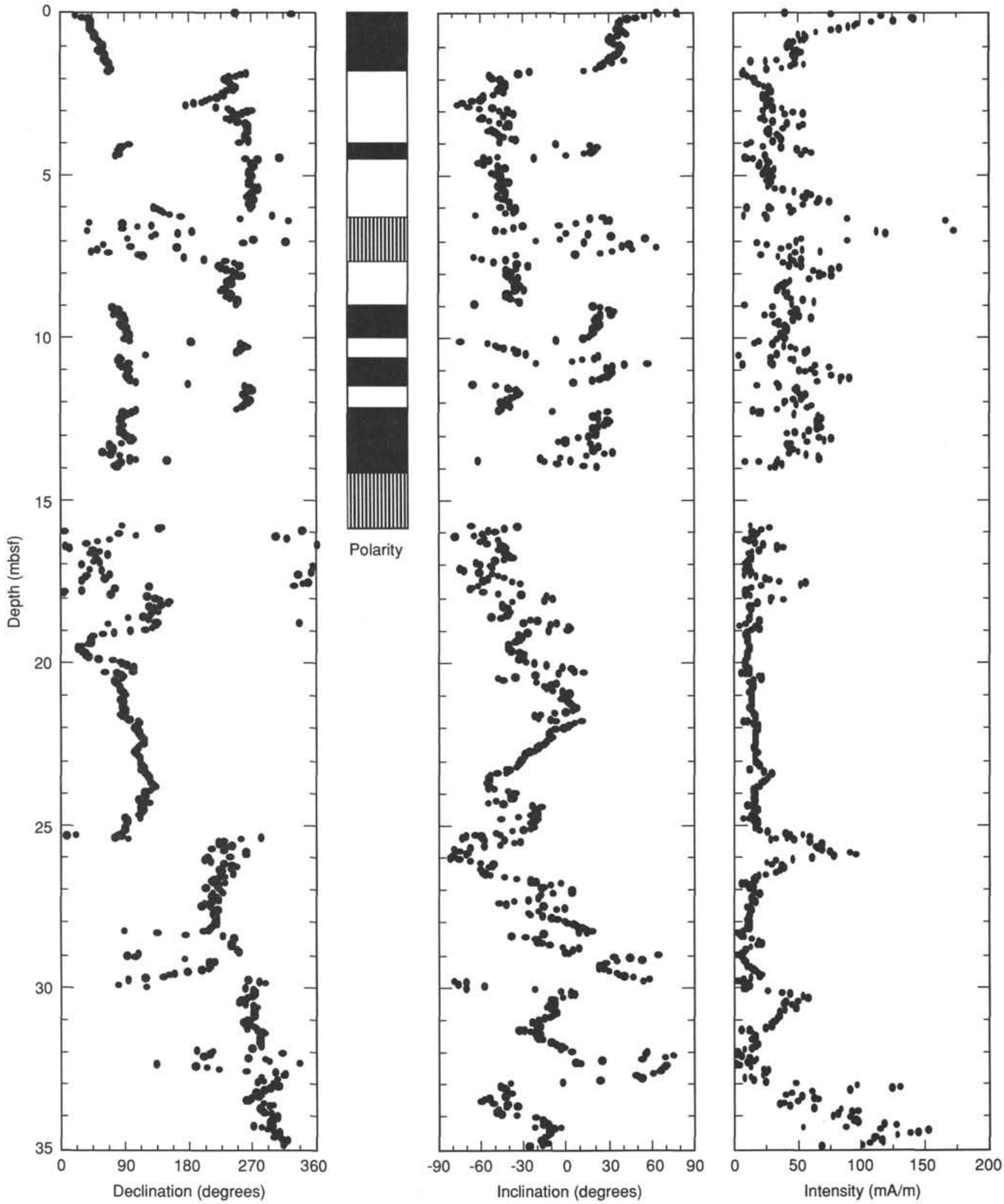

Figure 15. Plots of remanent magnetization (after AF demagnetization to 10 mT) vs. depth (mbsf) in Hole 136-842B; composite of Figures 11 to 14. Polarity indicated by black for normal, white for reversed; vertical lines for disturbed or missing intervals.

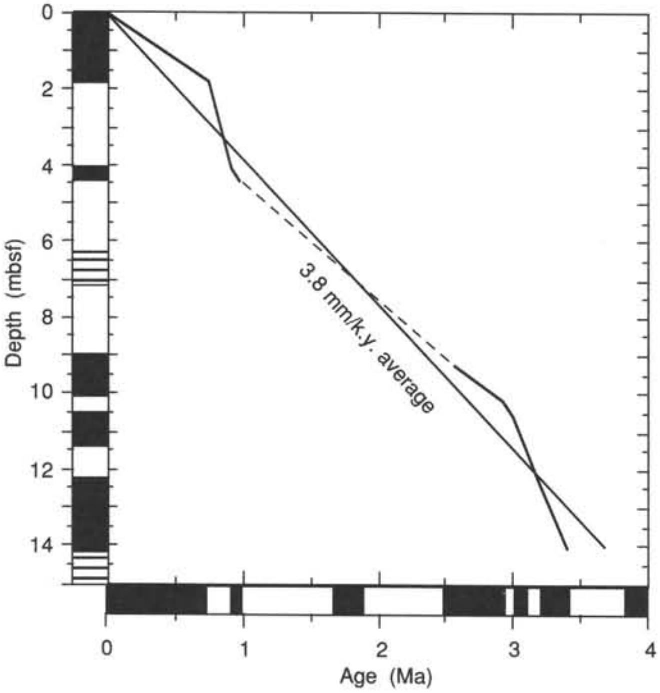

Figure 16. Interval-average sedimentation rates computed by comparison of the polarity stratigraphy of Hole 136-842B with the geomagnetic polarity time scale of Berggren et al. (1985).

taking place to a limited extent, except for Sample 136-842B-4H-5, 145–150 cm, which was potentially contaminated with seawater.

Phosphate

While PO_4^{3-} concentrations are low throughout the sediments of Site 842, a trend is nonetheless evident (Fig. 17). Concentrations of 2.5 to 3 μM occur near the top of Cores 136-842A-1H and 136-842B-1H, decrease to a minimum of 0.5 μM at 18.75 mbsf before they increase slightly to 1.1 μM at 32.75 mbsf. A possible explanation for the near-surface maximum is the preferential metabolism of phosphate by sulfate-reducing bacteria near the sediment/seawater interface as described by the following equation:

$$53\ SO_4^{2-} + C_{106}H_{263}O_{110}N_{16}P \rightleftarrows 39\ CO_2 + 67\ HCO_3^- + 16\ NH_4^+ + 53\ HS^- + 39\ H_2O + HPO_4^{2-}$$

Ammonium and Nitrate

Concentrations of NH_4^+ increase downhole (Fig. 17), but never exceed 0.15 mM. The NH_4^+ maximum corresponds roughly to the SO_4^{2-} minimum. Mirror image profiles are expected for these constituents because their concentrations are governed principally by the bacterially mediated oxidation of organic matter (i.e., the reaction given above), although data presented herein suggest that the stoichiometry of the above reaction is not adhered to.

The NO^{3-} profile, shown in Figure 17, is somewhat inconsistent with the behavior anticipated for this constituent. Nitrate levels are expected to initially remain constant down to the depth where O_2, used in the oxidation of organic matter, has been depleted. Subsequently NO^{3-}, a weaker electron acceptor than O_2, should begin to be reduced as it participates in the degradation of organic matter. Instead, the NO^{3-} concentration profile shows a small subsurface maximum near 50 μM in Interval 136-842A-1H-2, 145–150 cm, then decreases to much lower concentrations between 22 and 28 μM in the next two interstitial water samples (see Table 3 and Fig. 17). Subsequently, the NO_3^- concentration increases to 51.9 μM before decreasing gradually farther downhole. Whether the anomalous values are real or are artifacts due to sampling or analytical procedures remains uncertain. The NO_3^- profile downhole, however, is consistent with the reduction of this constituent to NO_2^- during the degradation of organic matter.

Calcium and Magnesium

Dissolved Mg^{2+} at Site 842 decreases slightly from 53 mM just below the sediment surface to 48.9 mM at 18.75 mbsf, whereas a small trend reversal to a concentration of 51.3 mM is observed over the next 9 m. Although only one deeper sample was obtained, its Mg^{2+} concentration is lower (50.5 mM).

Dissolved Ca^{2+} increases regularly from a near seawater value of 10.5 mM to 12.7 mM downhole and does not exhibit any gradient reversals. The generally antipathetic variation in these two constituents (Fig. 17), although the ratio of Mg loss to Ca gain is nearly 2:1, is suggestive of an exchange of Mg for Ca either during dolomitization or during the alteration of volcanic matter. The former is extremely unlikely because the sediments of Site 842, located considerably below the CCD, contain only trace amounts of calcium carbonate. The latter explanation is more plausible because alteration of volcanic matter, the presence of which has been confirmed by both the presence of ash layers and disseminated ash throughout the sediments of Site 842 (see "Lithostratigraphy" section, this chapter), results in the release of Ca and the removal of Mg from seawater. Such a pattern has been frequently observed in oceanic sediments (Gieskes, 1981). Furthermore, it is also likely that some Mg is taken up during reactions involving clay minerals, thereby accounting for the absence of a 1:1 exchange ratio for these metals. The nonlinear Mg/Ca vs. depth downhole relationship shown in Figure 17 is itself suggestive of reaction zones, and the possibility of several different reactions involving these elements.

Silica and Potassium

Dissolved silica profiles in deep-sea sediments generally reflect the local lithology of the sediments and the solubility of various phases. Additionally, silica gradients are often maintained to a much greater extent than those of other pore-water constituents. The common reaction sequence begins with the dissolution of the highly unstable opal-A phase (solubility of approximately 1 Mm), is followed by recrystallization to either opal-CT or quartz and subsequently by the recrystallization of opal-CT to the most stable phase, quartz (solubility of approximately 100 μM). Silica transformations are generally gradational with increasing sediment depth and depend both on temperature and sediment composition (Kastner, 1979). In the limited stratigraphic interval cored at Site 842, only the initial stages of this diagenetic progression are evident (Fig. 17). Although silica concentrations at Site 842 are substantially lower than observed at many other sites with pelagic sedimentation, dissolved silica concentrations in the sediments from the first core of Holes 842A and 842B are higher than observed in Cores 136-842B-2H and 136-842B-3H. The initial decrease in dissolved silica corresponds to the disappearance of radiolarians from the sediments (see "Biostratigraphy" section, this chapter) resulting from early diagenetic dissolution (Schrader, 1972). The subsequent sharp dissolved silica gradient is likely related to the conversion of opal-A to opal-CT, and corresponds to the first occurrences of chert in the sediments (see "Lithostratigraphy" Section, this chapter). Massive cherts were en-countered deeper downhole, although at relatively shallow depths (35 mbsf), as were found in early DSDP sites in this general area of the Pacific Ocean (e.g., DSDP Legs 6, 8, 17, 32, and 33).

Dissolved K^+ concentrations are all higher than expected for normal seawater and range between 11.3 mM and 12.8 mM

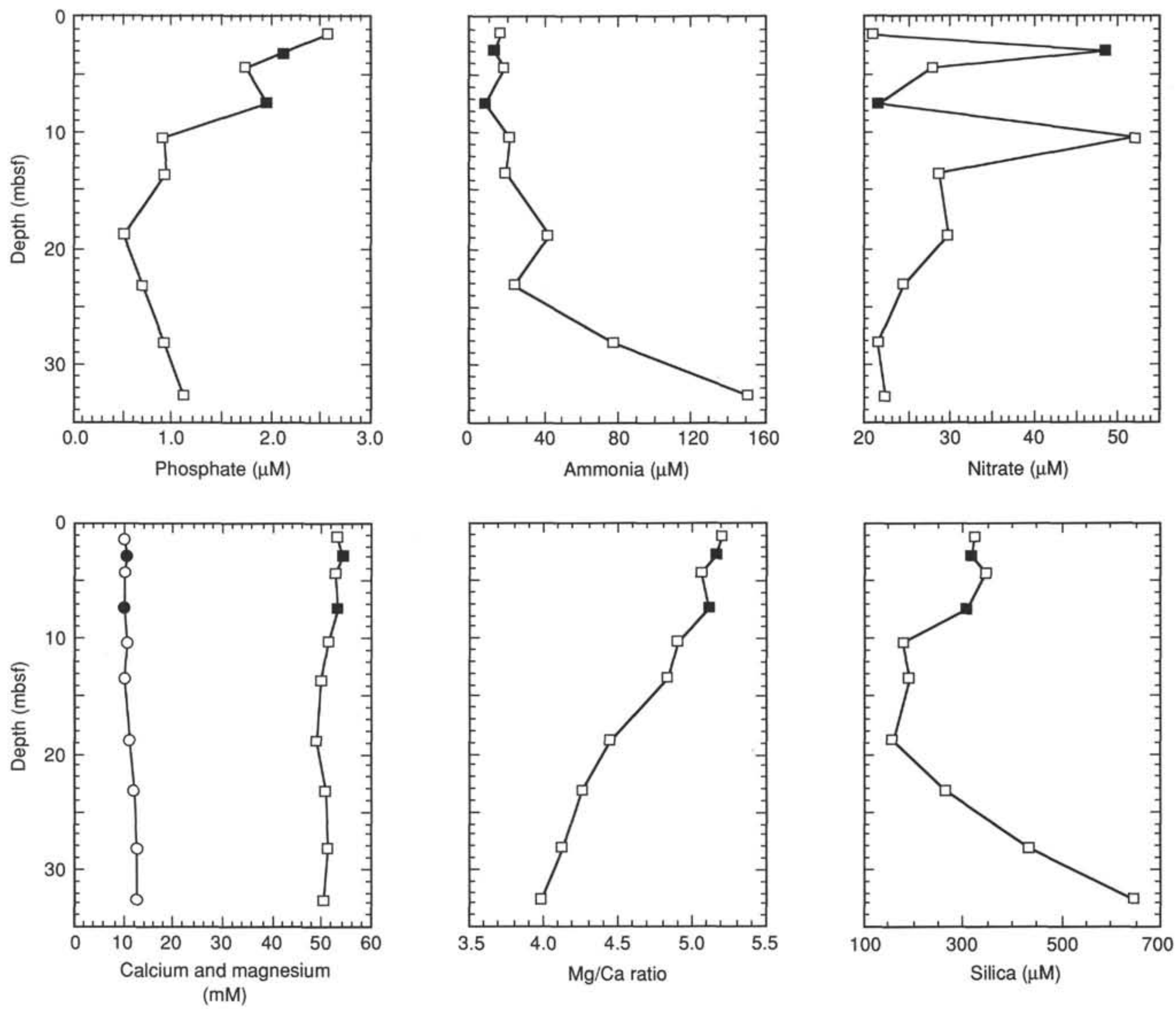

Figure 17. Concentration of PO_4^{3-}, NH_4^+, NO_3^-, CA^{2+}, and Mg^{2+}, Mg/Ca ratio, and Si as a function of depth downhole. Closed symbols: Hole 842A; open symbols: Hole 842B.

downhole, although no distinct trend is evident. The slightly elevated dissolved K^+ concentrations may be attributable to the well-known temperature of squeezing effect first described by Bischoff et al. (1970).

Conclusions

The limited depth of sampling precludes an in-depth interpretation of the diagenetic processes taking place in the red clay sediments of Site 842. Nonetheless, there is evidence of a limited extent of bacterially mediated oxidation of organic matter in the SO_4^{2-}, NH_4^+, and PO_4^{3-} pore-water profiles. Silica diagenesis, on the other hand, is well documented by the dissolved silica profile.

PHYSICAL PROPERTIES

Physical properties measured at Site 842 included index properties (water content, bulk density, and grain density, Table 4), *P*-wave sonic velocity, shear strength (Table 5), and thermal conductivity (Table 6). Techniques and equipment employed are delineated in "Physical Properties" section, Explanatory Notes Chapter. Holes 842A and 842B both encompass the uppermost 10 m of the sediment column and permit comparison of the physical properties in cores collected about 10 m apart.

Index Properties

In Hole 842A, major excursions in GRAPE bulk density (as high as 1.85 Mg/m^3) are associated with ash layers in Hole 842A (Fig. 18). The most obvious of these layers between 7 and 9.5 mbsf were not observed in Hole 842B, but generally high densities (1.35 Mg/m^3) in the same interval probably reflect the presence of disseminated ash. GRAPE Bulk densities in Hole 842B increase from values of about 1.3 Mg/m^3 near the surface to nearly 1.5 Mg/m^3 between 21–25 mbsf, and then decline to about 1.4 Mg/m^3 at the base of the cored section (35 mbsf; Fig. 19). Zones of anomalously high bulk density (>1.45 Mg/m^3) occur at depths of 2.5–3.5 mbsf and 10–18 mbsf, within the section comprised of silty clays, radiolarians, and volcanic ash. Between 18 and 30 mbsf, in the brown clay section, density is less variable and averages 1.47 Mg/m^3.

Table 4. Index properties (wet-bulk density, dry-bulk density, grain density, porosity, water content, void ratios) of discrete samples taken from Holes 842A and 842B.

Sample	Depth (mbsf)	Wet bulk density	Dry bulk density	Grain density	Porosity (%wet weight)	Water content (%wet weight)	Void ratio 1	Void ratio 2
136- 842A-								
1H-1, 35–37 cm	0.35	1.40	0.52	2.79	85.50	62.60	5.91	4.55
1H-1, 110–112	1.10	1.27	0.33	2.78	91.90	74.30	11.42	7.84
1H-2, 35–37	1.85	1.27	0.34	2.83	91.40	73.50	10.66	7.66
1H-2, 109–111	2.59	1.31	0.40	2.66	88.70	69.30	7.88	5.87
1H-3, 35–37	3.35	1.35	0.44	2.66	88.70	67.50	7.86	5.40
1H-3, 110–112	4.10	1.27	0.33	2.68	91.70	74.20	11.08	7.53
1H-4, 35–37	4.85	1.29	0.35	2.66	91.70	72.80	10.99	6.96
1H-4, 110–112	5.60	1.28	0.36	2.74	89.30	71.50	8.37	6.72
1H-5, 35–37	6.35	1.17	0.24	1.87	90.80	79.60	9.92	7.13
1H-5, 109–112	7.09	1.33	0.44	2.71	86.90	67.10	6.61	5.40
1H-6, 35–37	7.85	1.29	0.37	2.74	89.90	71.50	8.87	6.71
1H-6, 109–111	8.59	1.32	0.42	2.75	87.80	68.00	7.17	5.71
1H-7, 24–27	9.24	1.32	0.41	2.70	88.90	69.20	8.00	5.90
136-842B-								
1H-1, 35–37	0.35	1.37	0.49	2.78	85.70	64.10	6.01	4.84
1H-1, 110–112	1.10	1.25	0.31	2.51	91.40	74.90	10.62	7.33
1H-2, 35–37	1.85	1.26	0.33	2.61	90.00	73.50	9.02	7.06
1H-2, 110–112	2.60	1.43	0.58	2.71	82.90	59.60	4.84	3.90
1H-3, 35–37	3.35	1.28	0.35	2.74	91.30	72.90	10.49	7.18
1H-3, 110–112	4.10	1.28	0.36	2.70	90.30	72.10	9.32	6.82
1H-4, 35–37	4.85	1.28	0.36	2.83	90.40	72.10	9.37	7.15
1H-4, 110–112	5.60	1.29	0.38	2.70	89.40	70.70	8.43	6.37
2H-1, 110–112	7.40	1.37	0.49	2.74	86.10	64.30	6.17	4.81
2H-2, 35–37	8.15	1.36	0.50	2.70	83.70	63.20	5.14	4.52
2H-2, 110–112	8.90	1.32	0.42	2.71	87.40	68.00	6.95	5.61
2H-3, 35–37	9.65	1.30	0.40	2.74	87.90	69.30	7.29	6.03
2H-3, 110–112	10.40	1.31	0.42	2.73	86.40	67.70	6.35	5.60
2H-4, 35–37	11.15	1.38	0.50	2.75	85.40	63.60	5.85	4.68
2H-4, 110–112	11.90	1.35	0.44	2.75	88.90	67.50	8.00	5.57
2H-5, 35–37	12.65	1.31	0.42	2.84	87.00	68.10	6.68	5.90
2H-5, 110–112	13.40	1.30	0.40	2.65	87.30	68.90	6.89	5.73
2H-6, 11–13	13.91	1.28	0.37	2.63	89.10	71.40	8.13	6.40
3H-1, 35–37	16.15	1.41	0.57	2.71	82.90	60.00	4.85	3.97
3H-1, 110–112	16.90	1.51	0.64	3.42	85.00	57.60	5.68	4.53
3H-2, 35–37	17.65	1.40	0.54	2.78	84.30	61.60	5.39	4.35
3H-2, 110–112	18.40	1.36	0.51	2.70	82.60	62.20	4.76	4.33
3H-3, 35–37	19.15	1.40	0.54	2.74	84.30	61.60	5.36	4.29
3H-3, 110–112	19.90	1.41	0.56	2.73	82.80	60.20	4.80	4.03
3H-4, 35–37	20.65	1.47	0.64	2.66	80.80	56.50	4.21	3.37
3H-4, 110–112	21.40	1.45	0.62	2.71	81.00	57.20	4.28	3.53
3H-5, 35–37	22.15	1.43	0.60	2.68	81.00	57.90	4.27	3.60
3H-5, 110–112	22.90	1.44	0.61	2.58	80.40	57.40	4.10	3.40
3H-6, 35–37	23.65	1.37	0.60	2.67	75.60	56.40	3.10	3.36
3H-6, 110–112	24.40	1.44	0.62	2.66	80.40	57.10	4.11	3.46
3H-7, 49–51	25.29	1.36	0.60	2.55	73.80	55.80	2.82	3.14
4H-2, 110–113	27.90	1.37	0.60	2.66	75.80	56.60	3.13	3.38
4H-3, 35–38	28.65	1.36	0.59	2.71	74.40	56.20	2.91	3.40
4H-4, 35–37	30.15	1.38	0.59	2.65	76.90	57.10	3.33	3.43
4H-4, 110–112	30.90	1.37	0.58	2.65	77.60	57.90	3.47	3.56
4H-5, 35–37	31.65	1.36	0.53	2.58	80.70	60.70	4.17	3.89

Bulk densities determined by gravimetric and pycnometer analysis are systematically lower (by about 0.05 Mg/m^3) than the GRAPE densities. Periodic verification of the GRAPE and pycnometer calibrations suggests that the balance consistently provides artificially low sample weights.

Grain densities are relatively uniform at 2.7 Mg/m^3 above 18 mbsf, and then decline generally toward 2.6 Mg/m^3 at 32 mbsf (Fig. 20). Given the precision of the determinations (standard deviations associated with weighing and volume determinations are 0.043 g and 0.037 cm^3, respectively), the downhole change in grain density is statistically insignificant.

Index properties derived from the bulk density determinations (porosity, void ratio, water content) exhibit the normal compactive pattern of declining values downcore (Fig. 21), with excursions (as discussed previously) that may reflect subtle lithologic variations. The apparent increase in water content and porosity below 25 mbsf may represent coring disturbance.

Shear Strength

The sediment resistance to shear generally increases downcore in response to compactive dewatering. Shear strength is low near the surface (3–7 kPa) and attains maximum values (>37 kPa) between 29 and 31 mbsf (Fig. 22). Strength drops off markedly below 32 mbsf, probably due to disturbance related to coring. Comparison of shear strengths between Holes 842A and 842B indicates relatively high shear strengths in Hole 842A associated with the ash layers, but low values in Hole 842B. This disparity may suggest fabric disturbance between 6 and 10 mbsf in Hole 842B, although the sonic velocity profiles are strongly correlated (see below). Like the bulk density, the

Table 5. Shear strength of sediments in Holes 842A and 842B.

Core Section Interval (cm)	Depth (mbsf)	Shear strength (kPa)
136-842A-		
1H-1, 38–40	0.38	7.2
1H-1, 39–40	0.39	6.9
1H-1, 113–115	1.13	6.5
1H-2, 36–38	1.86	3.3
1H-2, 112–114	2.62	9.4
1H-3, 37–39	3.37	5.1
1H-3, 112–114	4.12	5.5
1H-4, 37–39	4.87	10.0
1H-4, 112–114	5.62	11.2
1H-5, 37–39	6.37	12.5
1H-5, 112–114	7.12	19.4
1H-6, 37–39	7.87	19.5
1H-6, 65–67	8.15	29.0
1H-6, 72–74	8.22	13.6
1H-6, 122–124	8.72	21.7
1H-6, 134–136	8.84	19.5
1H-7, 4–6	9.04	16.3
1H-7, 30–32	9.30	22.2
136-842B-		
1H-1, 42–44	0.42	5.5
1H-1, 112–114	1.12	2.2
1H-2, 37–39	1.87	9.2
1H-2, 112–114	2.62	10.4
1H-3, 37–39	3.37	13.9
1H-3, 112–114	4.1	11.42
1H-4, 37–39	4.87	11.2
1H-4, 114–116	5.64	13.9
1H-5, 4–6	6.04	9.6
2H-1, 112–114	7.42	3.3
2H-2, 37–39	8.17	10.8
2H-2, 112–114	8.92	7.6
2H-3, 32–34	9.62	9.0
2H-3, 112–114	10.42	10.0
2H-4, 37–39	11.17	20.4
2H-4, 106–108	11.86	22.7
2H-5, 37–39	12.67	27.6
2H-5, 112–114	13.42	22.2
2H-6, 14–16	13.94	15.0
3H-1, 37–39	16.17	6.3
3H-1, 112–114	16.92	24.5
3H-2, 14–16	17.44	8.2
3H-2, 112–114	18.42	6.3
3H-3, 37–39	19.17	16.8
3H-3, 112–114	19.92	14.5
3H-4, 37–39	20.67	17.2
3H-4, 112–114	21.42	15.9
3H-5, 42–44	22.22	23.6
3H-5, 112–114	22.92	24.0
3H-6, 37–39	23.67	26.3
3H-6, 112–114	24.42	25.8
3H-7, 22–24	25.02	28.1
3H-7, 52–54	25.32	27.2
4H-1, 112–114	26.42	23.1
4H-2, 37–39	27.17	26.7
4H-2, 112–114	27.92	33.1
4H-3, 37–39	28.67	36.7
4H-3, 112–114	29.42	37.2
4H-4, 37–39	30.17	37.2
4H-4, 112–114	30.92	37.2
4H-5, 37–39	31.67	34.9
4H-5, 69–71	31.99	35.3
4H-7, 19–21	34.49	9.5
4H-7, 39–40	34.69	6.3

Table 6. Thermal conductivity of sediments in Holes 842A and 842B.

Core Section Interval (cm)	Depth (mbsf)	Thermal conductivity (W/m/°C)
136-842A-		
1H-1, 79	0.79	0.71650
1H-3, 75	3.75	0.63020
1H-4, 75	5.25	0.70520
1H-6, 75	8.25	0.72870
136-842B-		
1H-1, 75	0.75	0.70730
1H-2, 75	2.25	0.83300
1H-3, 75	3.75	0.75140
1H-4, 75	5.25	0.76710
2H-1, 75	7.05	0.72940
2H-2, 75	8.55	0.73040
2H-5, 75	13.05	0.85700
3H-1, 75	16.55	0.90230
3H-3, 75	19.55	0.80640
3H-5, 75	22.55	0.88440
3H-6, 75	24.05	0.87560
4H-1, 75	26.05	0.80100
4H-4, 75	30.55	0.87310
4H-6, 75	33.55	0.79710

shear strength exhibits considerable variability above 19 mbsf, in the section marked by varying quantities of silt, clay, volcanic ash, and radiolarians. In the underlying clays, the strength increases uniformly from 7 to 37 kPa over an interval of 18 m.

Sonic Velocity

Compressional-wave (*P*-wave) velocities of material from Holes 842A and 842B were measured at intervals of about 2 cm using the multisensor track (MST) and at intervals of about 75 cm using the Hamilton Frame velocimeter. The measurement methodology is described in the "Explanatory Notes" chapter. The two independent data sets (Figs. 23 and 24) show similar variability as a function of depth. However, the data measured with the Hamilton Frame are greater in magnitude by about 2%–3%. This discrepancy can probably be attributed to incomplete calibration of the Hamilton Frame measurements (see "Explanatory Notes" chapter). Accordingly, the MST data are judged to be more reliable.

As one might expect for two cores separated laterally by about 10 m, the velocities of the first cores from Holes 842A and 842B are well correlated (Fig. 25). At depth, the Hole 842A sequence appears expanded by about 0.5 m relative to the Hole 842B sequence. While this offset may have a geological explanation, it might also be a result of incomplete core recovery. It is interesting to note that comparison of the bulk density profiles over the same interval does not show as good a correlation as the velocity data. Clearly, density—and indirectly porosity—is not always the primary control on velocity.

The relatively large downhole variability in the upper 19 m of Hole 842B is associated with the variable nature of lithologic Unit I. In particular, the high velocity layers correlate with the presence of volcanic ash. At greater depth, the velocities of the brown clays are more uniform.

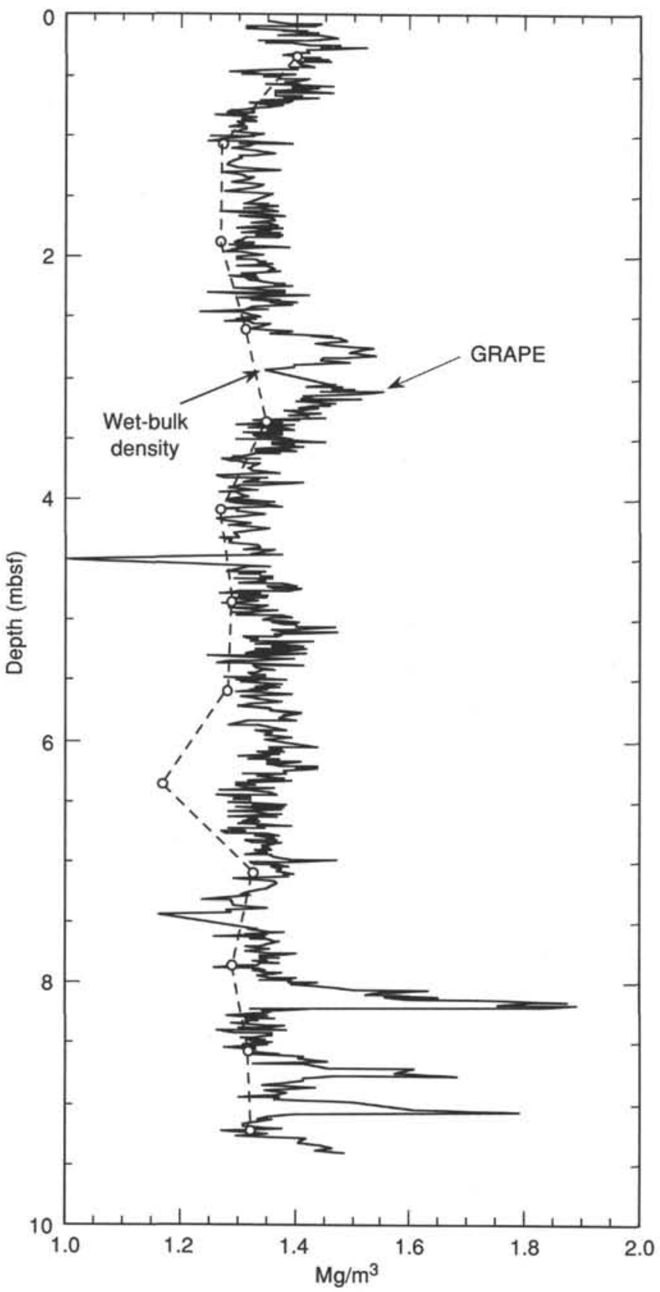

Figure 18. Bulk density determinations for Hole 842A, by GRAPE and discrete sample determinations. GRAPE values as plotted are 5-point moving averages to remove high-frequency variability.

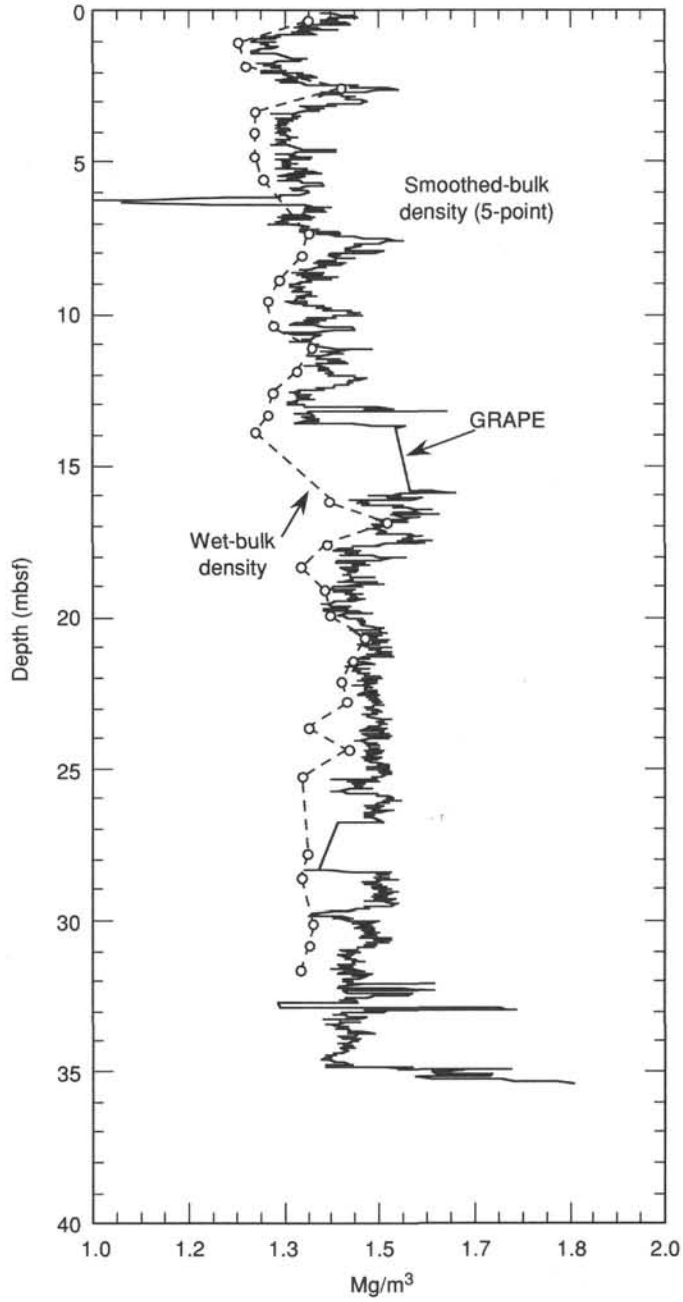

Figure 19. Bulk density determinations for Hole 842B, by GRAPE and discrete sample determinations. GRAPE values as plotted are 5-point moving averages to remove high-frequency variability.

Thermal Conductivity

Thermal conductivities were measured at one location in each core section using the full space method (Von Herzen and Maxwell, 1959). Although the data are sparse (Figs. 26 and 27), the measured values correlate with downhole variations in porosity as one might expect. It is not known why the values for Hole 842A are lower in magnitude than those for Hole 842B.

REFERENCES

Berggren, W. A., Kent, D. V., Flynn, J., and Van Couvering, J. A., 1985. Cenozoic geochronology. *Geol. Soc. Am. Bull.*, 96:1407–1418.

Bischoff, J. L., Greer, R. E., and Luistro, A. O., 1970. Composition of interstitial waters of marine sediments: temperature of squeezing effect. *Science*, 167:1245–1246.

Doyle, P. S., and Riedel, W. R., 1979. Cretaceous to Neogene ichthyoliths in a giant piston core from the central North Pacific. *Micropaleontology*, 25:337–364.

———, 1985. Cenozoic and Late Cretaceous ichthyoliths. *In* Bolli, H. M., Saunders, J. B., and Perch-Nielsen, K. (Eds.), *Plankton Stratigraphy:* Cambridge (Cambridge Univ. Press), 965–994.

Gieskes, J. M., 1981. Deep-sea drilling interstitial water studies: implications for chemical alteration of the oceanic crust, layers I and II. *In* Warme, J. E., Douglas, R. G., and Winterer, E. L. (Eds.), *The Deep Sea Drilling Project: A Decade of Progress*. Soc. Econ. Paleontol. Mineral. Spec. Publ., 32:149–167.

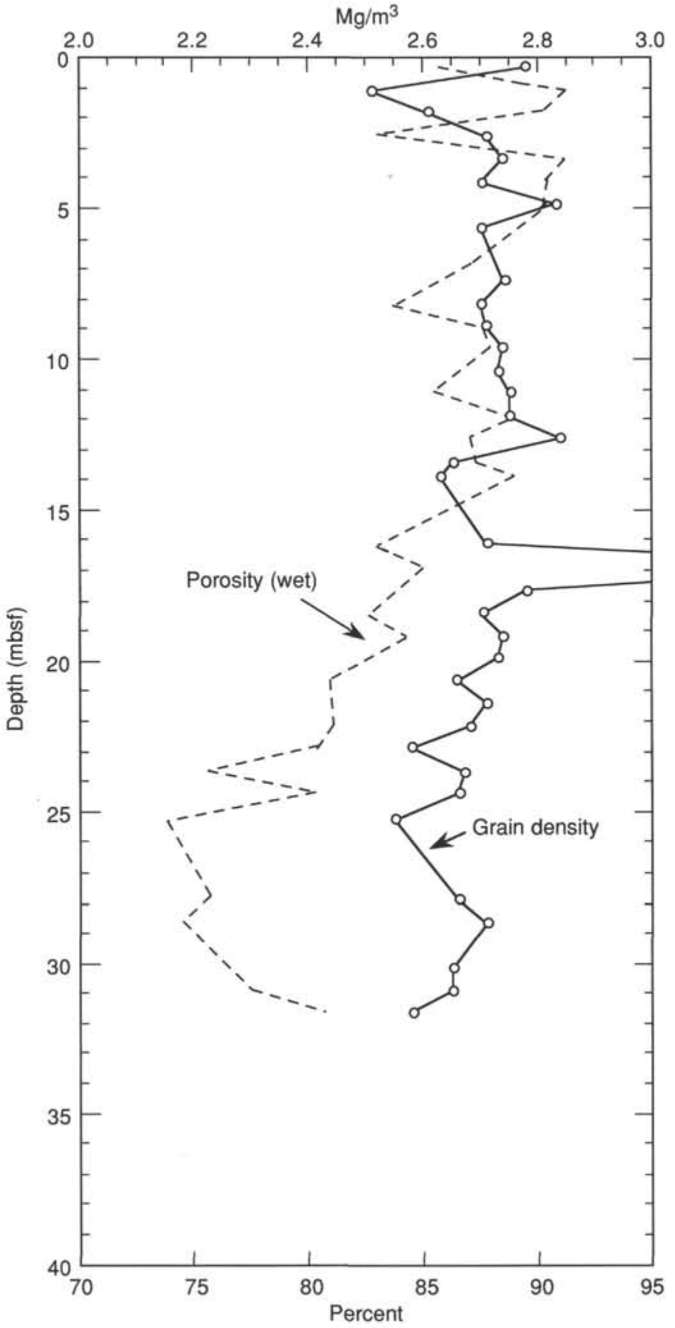

Figure 20. Porosity (% wet weight) and grain density determined on discrete samples at Hole 842B.

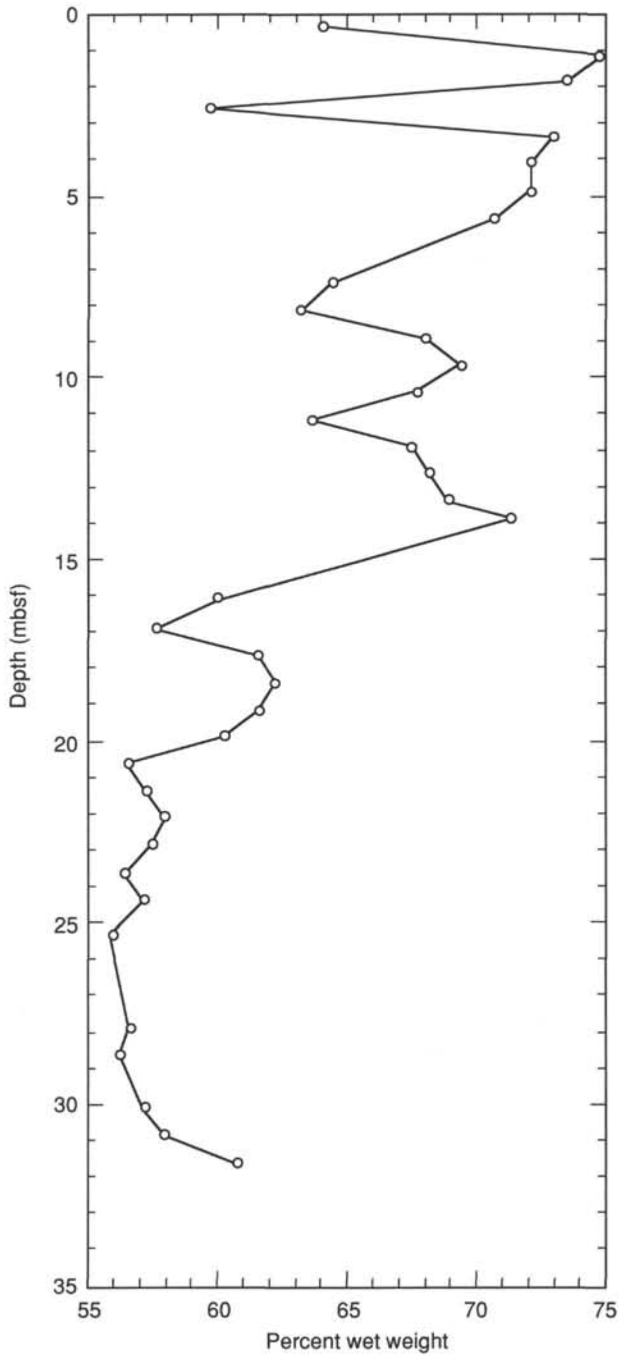

Figure 21. Water content (% wet weight) distribution at Hole 842B.

Kastner, M., 1979. Silica polymorphs. *In* Burns, R. G. (Ed.), *Marine Minerals:* Miner. Soc. Am. Rev. Miner., 6:99–111.

Sanfilippo, A., Westberg-Smith, M. J., and Riedel, W. R., 1985. Cenozoic radiolaria. *In* Bolli, H. M., Saunders, J. B., and Perch-Nielsen, K. (Eds.), *Plankton Stratigraphy:* Cambridge (Cambridge Univ. Press), 631–712.

Schrader, H.-J., 1972. Kieselsaure-Skelette in sedimenten des ibero-marokkanischen Kontinentalrandes und angrendzender Tiefsee Ebenen. *"Meteor" Forschungsergeb. Reihe C,* 8:10–36.

Von Herzen, R. P., and Maxwell, A. E., 1959. The measurement of thermal conductivity of deep-sea sediments by a needle probe method. *J. Geophys. Res.,* 65:1557–1563.

Ms 136A-104

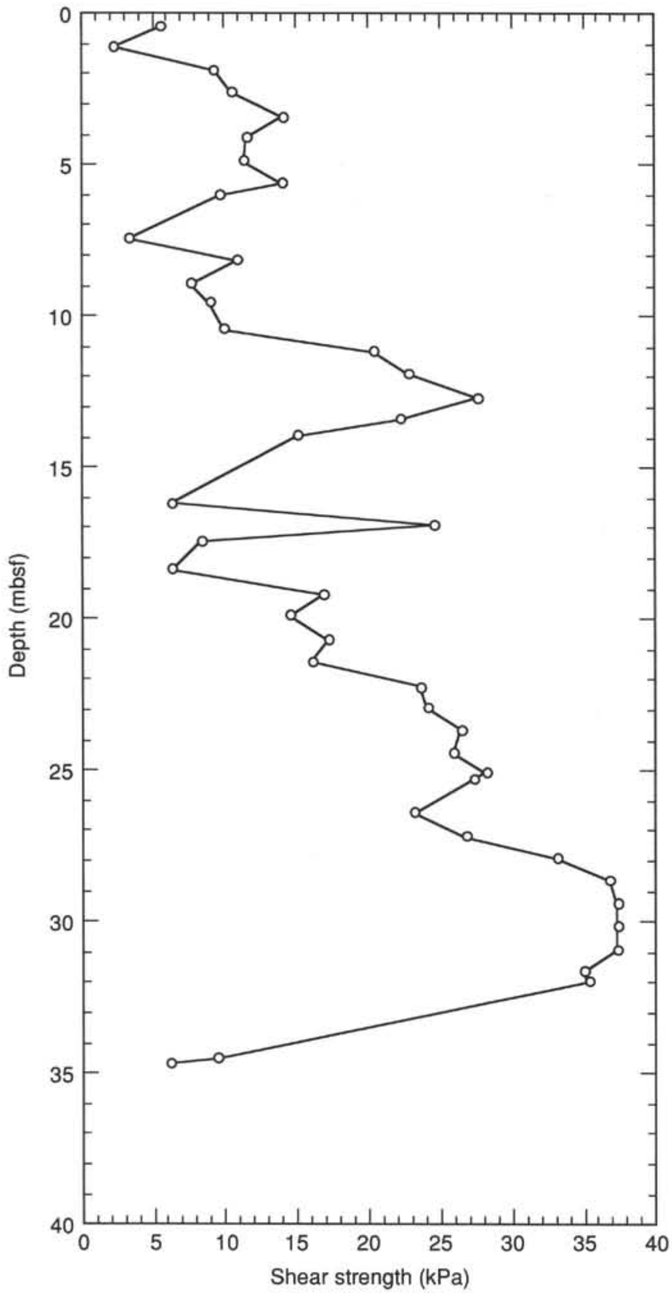

Figure 22. Vane shear as a function of depth at Hole 842B.

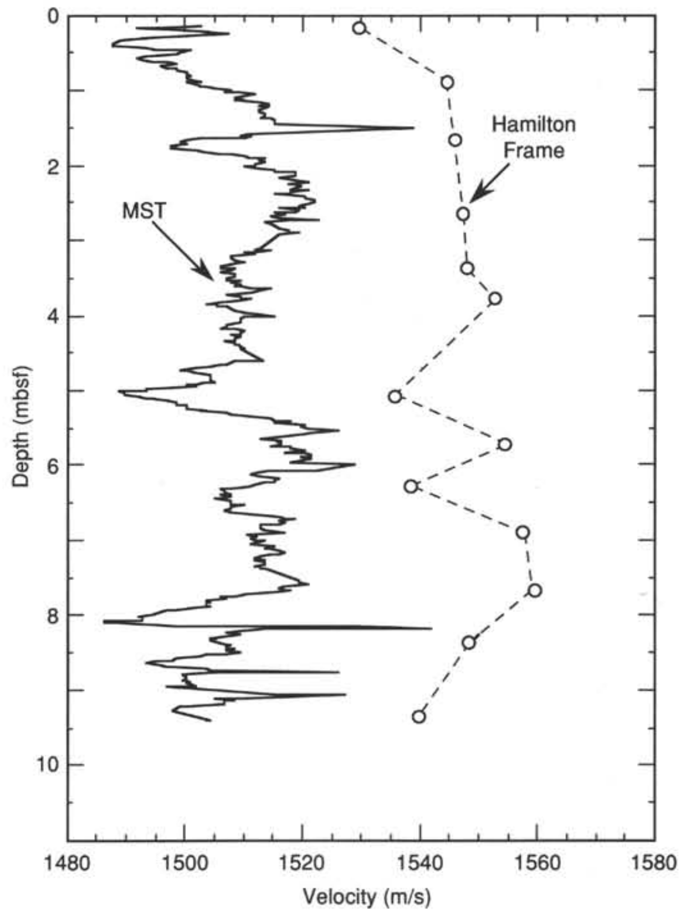

Figure 23. Velocity as a function of depth for Hole 842A.

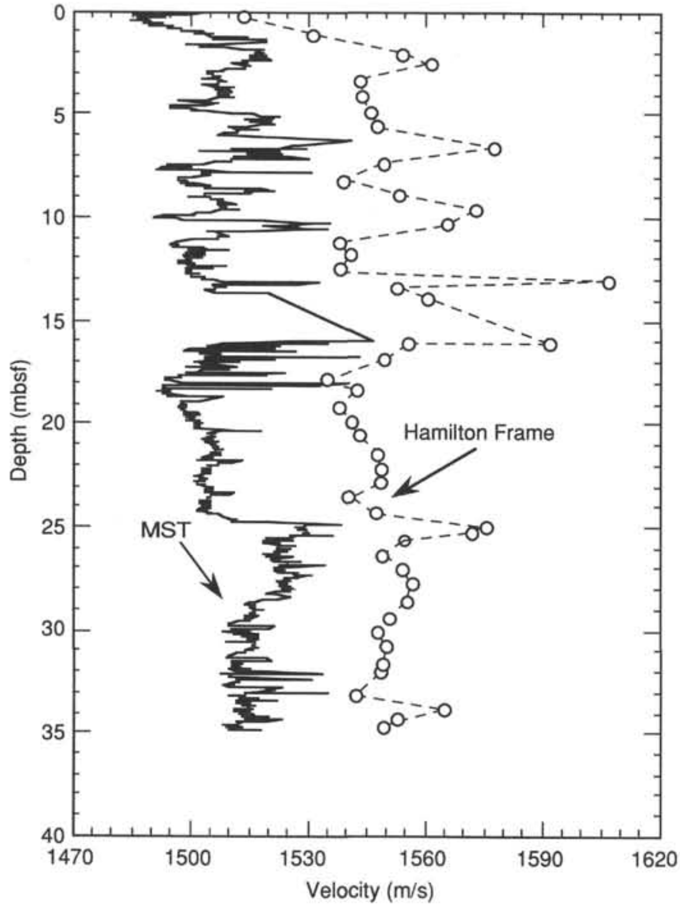

Figure 24. Velocity as a function of depth for Hole 842B.

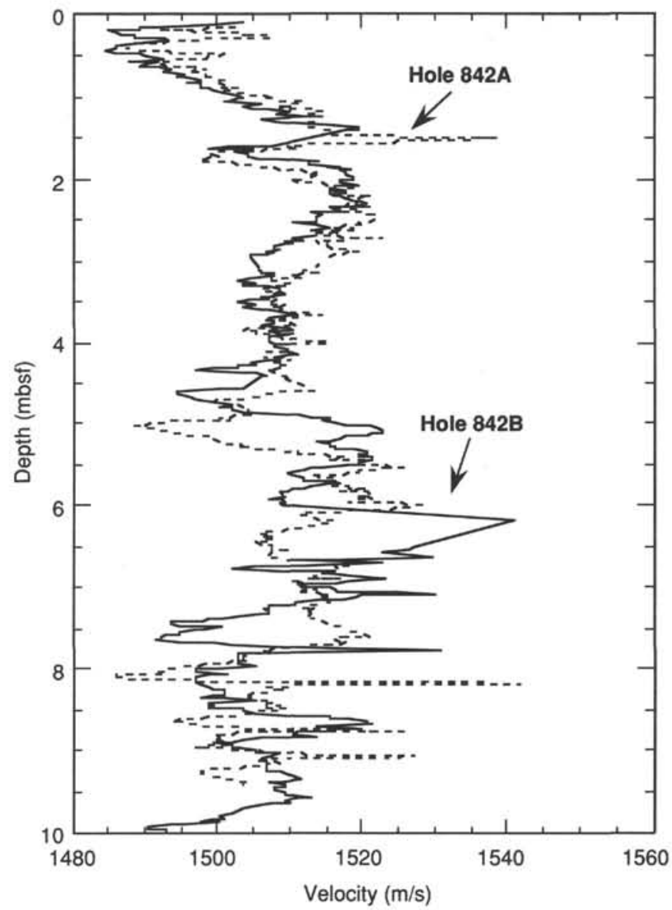

Figure 25. Comparison of the velocity data for Holes 842A and 842B. Both data sets were measured using the MST.

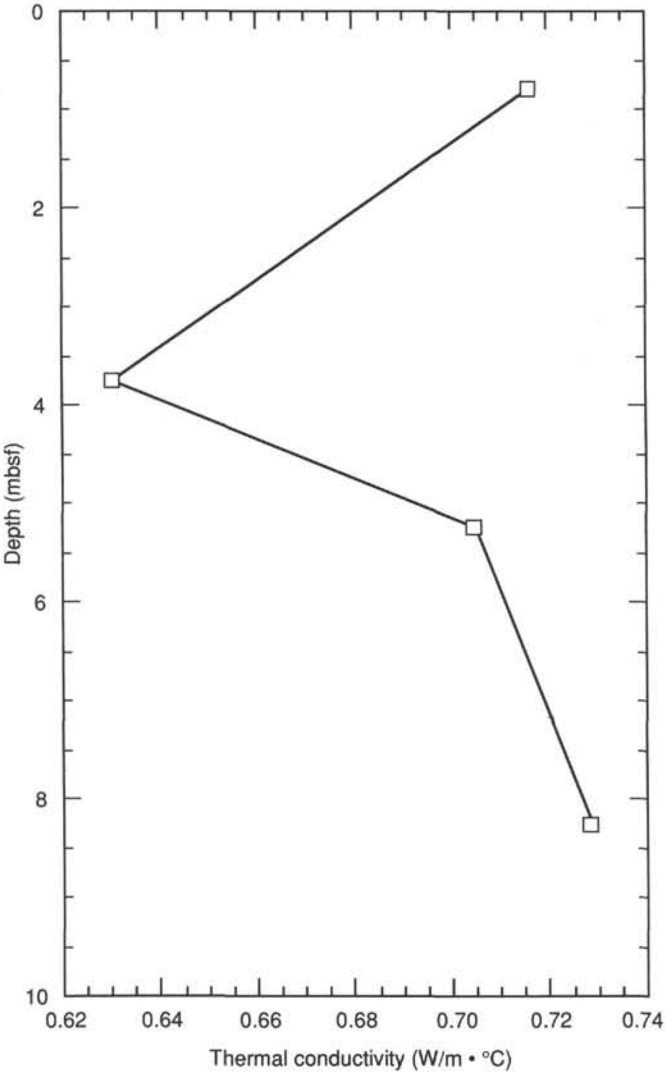

Figure 26. Thermal conductivity as a function of depth for Hole 842A.

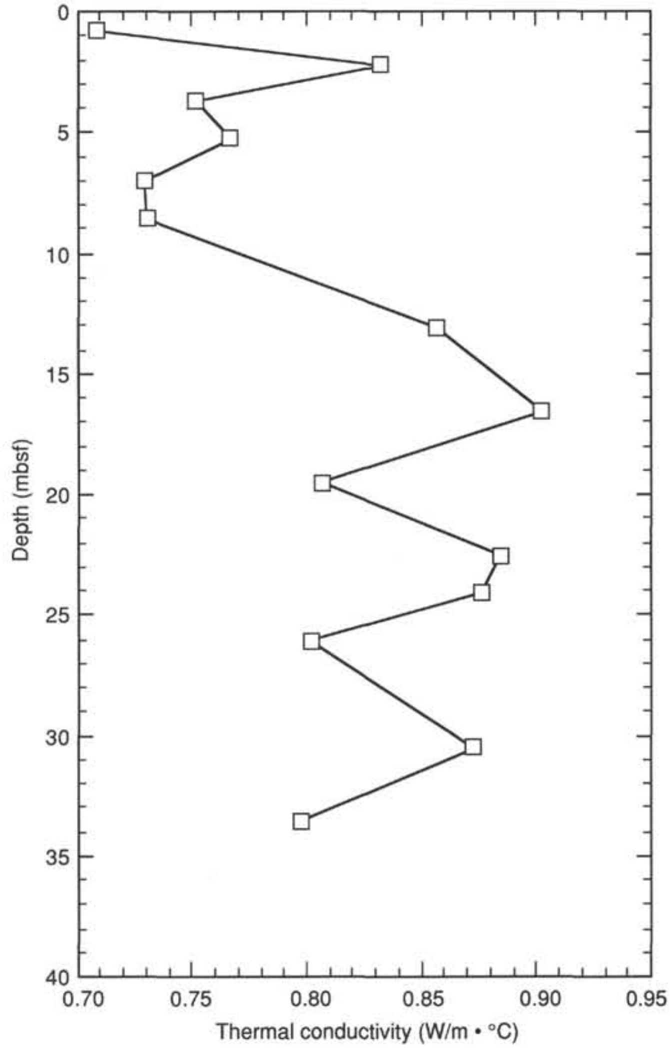

Figure 27. Thermal conductivity as a function of depth for Hole 842B.